

Registration for Incomplete Non-Gaussian Functional Data

Alexander Bauer*

Department of Statistics, Ludwig-Maximilians-Universität, Munich, Germany
and

Fabian Scheipl

Department of Statistics, Ludwig-Maximilians-Universität, Munich, Germany
and

Helmut Küchenhoff

Department of Statistics, Ludwig-Maximilians-Universität, Munich, Germany
and

Alice-Agnes Gabriel

Department of Earth and Environmental Sciences,
Ludwig-Maximilians-Universität, Munich, Germany

Abstract

Accounting for phase variability is a critical challenge in functional data analysis. To separate it from amplitude variation, functional data are registered, i.e., their observed domains are deformed elastically so that the resulting functions are aligned with template functions. At present, most available registration approaches are limited to datasets of complete and densely measured curves with Gaussian noise. However, many real-world functional data sets are not Gaussian and contain incomplete curves, in which the underlying process is not recorded over its entire domain. In this work, we extend and refine a framework for joint likelihood-based registration and latent Gaussian process-based generalized functional principal component analysis that is able to handle incomplete curves. Our approach is accompanied by sophisticated open-source software, allowing for its application in diverse non-Gaussian data settings and a public code repository to reproduce all results. We register data from a seismological application comprising spatially indexed, incomplete ground velocity time series with a highly volatile Gamma structure. We describe, implement and evaluate the approach for such incomplete non-Gaussian functional data and compare it to existing routines.

*This work was supported by the German Research Foundation (DFG) under Grant KU 1359/4-1; and the German Federal Ministry of Education and Research (BMBF) under Grant No. 01IS18036A.

Keywords: functional data analysis; phase variability; amplitude variability; curve alignment; partially observed curves; seismology.

1 Introduction

Dealing with phase variability is crucial in functional data analysis. Many different approaches exist for registering curves (see e.g. Marron et al., 2015), but their application to diverse real world data settings remains challenging. Most existing approaches target small to intermediate datasets of completely observed curves with small amounts of Gaussian noise, evaluated on dense, regular grids. Especially the registration of *incomplete* curves, i.e., curves whose underlying process is not observed from its natural starting point all the way to its natural endpoint, has received only limited attention so far (see e.g. Matuk et al., 2019; Bryner and Srivastava, 2021). However, such data arise in many fields. Missing information about the initial development of some processes, i.e. *leading incompleteness*, can be caused by different starting conditions of subjects at the beginning of a study. *Trailing incompleteness* towards the end of the underlying processes is present in experiments and studies with a fixed endpoint that causes right-censoring, or in panel studies with relevant dropout rates. If both types of incompleteness are present, we use the term *full incompleteness*.

— Notation

In this functional data setting, we observe discretized incomplete curves $Y_i(t_i^*)$, $i = 1, \dots, N$ over individual *chronological time domains* T_i^* , where the observed grids $\mathbf{t}_i^* = [t_{ij}^*]_{j=1, \dots, n_i}$ may be irregular or sparse, and chronological domains $T_i^* = [t_{\min, i}^*, t_{\max, i}^*]$ are defined by the individual observation periods. W.l.o.g. we assume that all observed curves are realizations of stochastic processes over a common underlying *internal time domain* $T = [0, 1]$ and $T_i^* \subseteq T \ \forall i$. Registering the curves requires estimating inverse warping functions $h_i^{-1} : T_i^* \mapsto T$ that account for the data’s phase variation and map individual chronological times to the internal time of the underlying process. The resulting registered curves $Y_i(t) = Y_i(h_i^{-1}(t_i^*))$ only contain amplitude variation.

Applying conventional “complete curve” registration methods to incomplete curves often leads to nonsensical results (see Figure 1). This is caused by the implicit, unwarranted assumption that the endpoints of the individual observed chronological domains T_i^* are identical to those of the global internal time domain T .

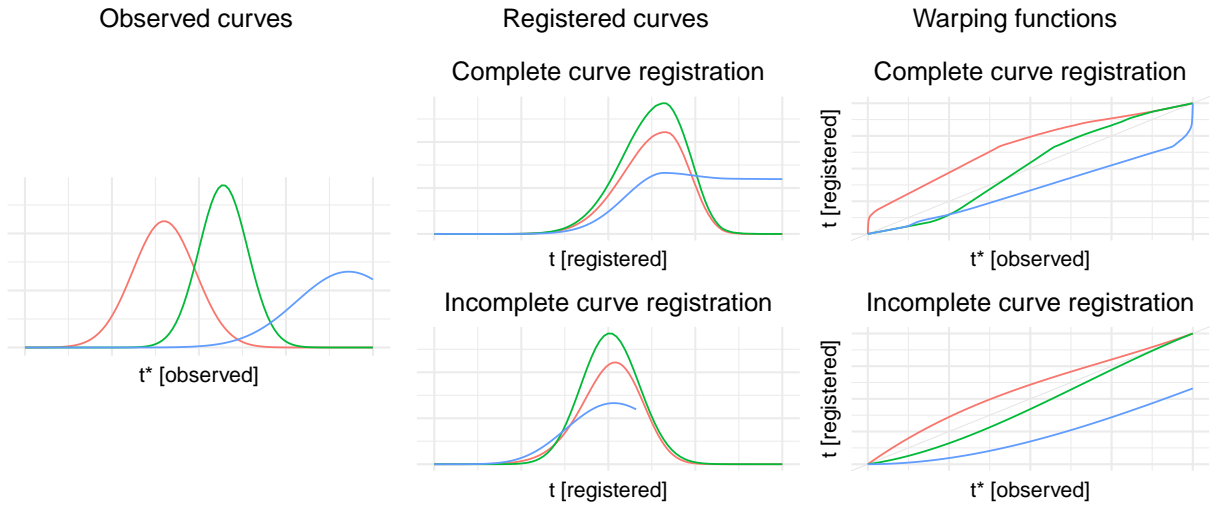


Figure 1: Simulated observed curves with trailing incompleteness (left column), registered curves only comprising amplitude variation (center), and inverse warping functions visualizing phase variation (right). Registration was performed with the complete curve SRVF approach of Srivastava et al. (2011) with function `time_warping()` from the R package `fdasrvf` (top row; Tucker, 2020) and our incomplete curve approach (bottom row). Note the extreme time dilation around the blue curve’s peak in the top row, which yields a highly implausible registered curve.

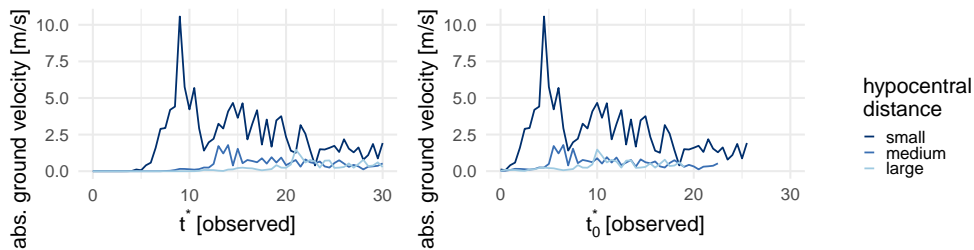


Figure 2: Typical seismic observations recorded at different hypocentral distances. As a preprocessing step, the leading zero measurements of the raw curves (left pane) are cut off and absolute ground velocities are analyzed on the *time since the first relevant absolute ground velocity measurement* t_0^* (right).

— Data setting

Our approach is motivated by synthetic seismic data originating from large-scale numerical *in silico* experiments based on the 1994 magnitude 6.7 earthquake in Northridge (California). The experiments were performed by the Department of Earth and Environmental Sciences (LMU Munich, Germany) using the software SeisSol (Pelties et al., 2014; Uphoff et al., 2017, github.com/SeisSol/SeisSol) and are used to assess critical geophysical parameters associated with high ground motion in the event of an earthquake. The simulated ground motion curves contain highly relevant phase variation due to different propagation velocities of the seismic waves and their varying distance to the hypocenter of the earthquake. The complete data comprise 800 000 curves, each recorded over 30 seconds with a frequency of 2Hz. Seismic activity has not subsided after 30 seconds in many cases, so the curves are mostly incomplete. For more information on the data setting see Bauer et al. (2017), Bauer et al. (2018) and Happ et al. (2019). In order to investigate the structure of phase and amplitude variability of these highly variable and spatially indexed data, we register them to spatially varying template functions learnt from the data and represent the registered curves in a lower-dimensional space. Note that these data do not have a simple structure with additive Gaussian noise since absolute ground motion velocities are nonnegative and higher values entail higher variability (see Figure 2).

We also apply our method to a version of the well-known Berkeley child growth study data (Ramsay and Silverman, 2005). The data contain annual measurements of the body heights of 39 boys and 54 girls from ages 1 to 18. The focus lies on the first derivatives of the data, i.e., the speed of growth in different stages of childhood and adolescence. We simulate full incompleteness in these data by drawing an artificial initial age for every child in the first quarter of the time domain as well as an individual drop-out year in the second half of the domain. The observed curves with simulated incompleteness are visualized in Figure 6.

— Study aim and contributions

Motivated by the challenges inherent in the seismic data, we require a curve registration method that (i) is able to handle incomplete curves, (ii) is applicable to non-Gaussian

data and (iii) includes a lower-dimensional representation of the registered curves. The latter is especially of interest for further analyses of the estimated phase and amplitude variation structure. To achieve these goals, we (i) derive and implement a novel penalized approach for incomplete data registration and (ii, iii) derive and implement extensions of the methods introduced by Wrobel et al. (2019) for exponential family distributions beyond Binomial and Gaussian data. Furthermore, we implement multiple computational improvements in the underlying software stack to accelerate and stabilize the algorithm. Our implementation is available in the `registr` package (Wrobel and Bauer, 2021) for the open-source software R (R Core Team, 2020). All analyses in this paper can be reproduced based on the code and data in our public GitHub repository (Bauer, 2021).

Before introducing our method in Section 3 we give an overview of prior work in Section 2. Sections 4 and 5 comprise an extensive simulation study and the applications. We end with a discussion in Section 6.

2 Related Work

2.1 Registration

Accounting for phase variation is often critical when analyzing functional data. We refer to Marron et al. (2015) and the references therein for an introduction to the general issue and a detailed overview of available registration approaches. Many early approaches focused on the alignment of curves towards given (salient) structures, i.e., landmark registration (e.g. Kneip and Gasser, 1992). More recent proposals mostly perform alignment towards *template functions* that are either based on domain knowledge or estimated based on some measure of centrality, with such estimates often iteratively refined over the course of the registration procedure. Warping functions are commonly estimated purely nonparametrically (e.g. Chakraborty and Panaretos, 2017; Tucker, 2020), as (piecewise) linear functions (e.g. Sangalli et al., 2010; Vitelli, 2019; McDonnell et al., 2021) or in a basis expansion. Common examples for the latter are the use of (penalized) B-spline (Telesca and Inoue, 2008; Wrobel et al., 2019) or Fourier (Mattar et al., 2009) bases or of warplets (Claeskens

et al., 2010).

— SRVF-based registration approaches

One of the most popular approaches is the square-root velocity function (SRVF) framework introduced by Srivastava et al. (2011), who showed that the warping-invariant Fisher-Rao metric quantifies pure amplitude distances and is equivalent to the simple L_2 -metric in the SRVF space. Recently, Guo et al. (2020) have extended this framework to jointly analyze amplitude, phase and spatial variation.

Cheng et al. (2016), Kurtek (2017) and Lu et al. (2017) adapted the SRVF approach to perform registration in a Bayesian setting. Bayesian approaches were also introduced for data settings with stronger noise under informative priors (Matuk et al., 2019; Tucker et al., 2021). These Bayesian approaches can provide a full representation of the joint phase and amplitude uncertainty, but are computationally very demanding. The method of Matuk et al. (2019) handles sparse and fragmented Gaussian functional data where measurements are only available over some parts of the observation domain, but no software implementation was publicly available at the time of writing.

More recently, Nunez et al. (2021) and Chen and Srivastava (2021) introduced the neural network-based frameworks SrvfNet and SrvfRegNet, respectively. Both approaches build on the SRVF framework and enable a highly efficient estimation and prediction of warping functions in large-scale data settings for registering curves to their Karcher mean or fixed and pre-specified template functions.

— Other registration approaches

All the above approaches are limited to continuous functional data, mostly under the assumption of Gaussian errors. Some extensions to binary functional data such as Wu and Srivastava (2014) and Panaretos and Zemel (2016) rely on a pre-smoothing step to obtain a continuous representation of the curves. The *congealing* approach of Learned-Miller (2005) (adapted to functional data by Mattar et al., 2009), which iteratively optimizes measures of alignment like the integrated point-wise differential entropy via gradient descent, is applicable in diverse data situations and computationally efficient. Wrobel et al. (2019) utilizes a likelihood-based optimization approach for exponential family data which is able

to practically handle moderate-to-large scale datasets (Wrobel et al., 2021).

— Joint registration and low-rank representations

For analyzing the main modes of amplitude and phase variation, it is common to estimate a low-rank representation of the registered curves or, at least, the template functions that serve as registration targets, and potentially also of the estimated warping functions. Tucker et al. (2013), Hadjipantelis et al. (2015), Lee and Jung (2016) and Happ et al. (2019) use (joint) functional principal component analysis (FPCA) for finding compact representations of both phase and amplitude modes of variation.

Tucker (2014) (utilizing the SRVF approach of Srivastava et al., 2011, for registration), Wagner and Kneip (2019) and Kneip and Ramsay (2008) (optimizing a least squares criterion) and Wrobel et al. (2019) (optimizing an exponential family likelihood) all utilize iterative algorithms to successively refine warping functions that lead to registered curves whose amplitude variation can be represented in terms of a low-rank FPC basis.

— Incomplete curve registration

Comparatively few approaches have been developed so far for the registration of incomplete curves. Some heuristic approaches are available in the field of dynamic time warping (DTW) for time series analysis. Subsequence DTW offers a framework to find a subsequence of a (fully observed) template curve to which a partially observed curve can be matched (see Müller, 2015, 7.2). Tormene et al. (2009) introduce an algorithm for “open-begin and open-end” DTW (OBE-DTW) that is also able to handle full incompleteness.

More sophisticated registration approaches were introduced only recently. Sangalli et al. (2010) and Vitelli (2019) make use of linear warping functions with free starting points and endpoints. The observed curve domains are constrained so that they dilate or extend the domain by a factor $0.9 - 1.1$ to ensure reasonable warpings. As noted above, Matuk et al. (2019) allows to analyze fragmented functional data, but their approach is feasible only for small to intermediate sets of Gaussian data.

Bryner and Srivastava (2021) introduced an approach for *elastic partial matching* to tackle trailing incompleteness. Before registering each curve to its template using the complete curve SRVF approach of Srivastava et al. (2011) they estimate the time scaling

necessary to (partially) match the observed domain of a specific curve to the domain of the template curve and perform the registration only on the intersection of the curves' domains. Both steps are combined in a joint, gradient-based algorithm. At the time of writing, no implementation of their method was available on request.

— Software implementations

Multiple packages for the statistical open-source software R (R Core Team, 2020) exist that implement registration approaches. Basic approaches outlined in Ramsay and Silverman (2005) are implemented in package `fda` (Ramsay et al., 2020). The OBE-DTW approach of Tormene et al. (2009) is available in `dtw` (Giorgino, 2009). Package `fdasrvf` (Tucker, 2020) implements the SRVF registration of Srivastava et al. (2011) and the iterative procedure of Tucker (2014) for finding overall similar registered curves with a low-rank FPCA representation. Code for Wagner and Kneip (2019) is available on GitHub (Wagner, 2020). R package `registr` (Wrobel and Bauer, 2021) implements the likelihood-based approach of Wrobel et al. (2019) and the incomplete curve extensions presented in this work for various exponential family distributions.

2.2 Generalized Functional Principal Component Analysis

Functional principal component analysis (FPCA) is a technique to analyze and represent functional data in terms of their main modes of variation (Ramsay and Silverman, 2005). To purely represent amplitude variation, FPCA is most commonly applied to curves without phase variation, potentially after an initial registration step. As noted above, the concept of FPCA was also extended to separately (Tucker et al., 2013) or simultaneously (Happ et al., 2019) analyze amplitude and phase variation. Multiple approaches exist for FPCA on sparse or partially observed functional data, but mostly assume Gaussianity (c.f. Stefanucci et al., 2018). Adaptations to the non-Gaussian case for performing generalized FPCA (GFPCA) do exist, but have to be assessed with care since marginal estimation of the overall mean can introduce bias (Gertheiss et al., 2017).

— Probabilistic GFPCA

A popular method for multivariate non-Gaussian data is *probabilistic FPCA* (Tipping and

Bishop, 1999), based on likelihood optimization. For the case of Gaussian functional data, James et al. (2000) and Rice and Wu (2001) use a similar approach based on mixed-effects regression. Zhou et al. (2008) adapted these methods in a paired-curve setting. Huang et al. (2014) extended the ideas of James et al. (2000) and Zhou et al. (2008) to non-Gaussian functional data and combined them with a clustering approach. Recently, Wrobel et al. (2019) further adapted the mixed model-based approach by introducing a link function and estimating the GFPCA based on computationally efficient variational approximations. To the best of our knowledge, efficient approximations are available only for Gaussian and binary data and are not directly adaptable to further exponential family distributions.

Bayesian adaptations of probabilistic FPCA to non-Gaussian settings were introduced by van der Linde (2009) for binary and count data, and Goldsmith et al. (2015) with an extension to multilevel data. While these Bayesian approaches can provide a full representation of the underlying uncertainty and show good performance in sparse data situations (c.f. Gertheiss et al., 2017), they are computationally demanding.

— Two-step GFPCA

A nonparametric approach to Gaussian FPCA was introduced by Yao et al. (2005) and adapted by Hall et al. (2008) for the non-Gaussian case. Serban et al. (2013) extended this method to further handle multilevel binary data with potentially rare events. Li and Guan (2014) used a similar approach to model point processes with a spatio-temporal correlation structure. Gertheiss et al. (2017) showed that the marginal mean estimates proposed by Hall et al. (2008) can introduce bias in non-Gaussian data settings and tackled this issue by plugging the eigenfunction estimates into a generalized additive mixed model to achieve an estimation of the mean structure conditional on FPC scores represented as random effects.

— Some notes on consistency

Consistent estimators for the covariance operator are crucial for FPCA. The consistency and convergence rates of estimators for covariance operators were thoroughly studied for differently dense data settings (c.f. Wang et al., 2016; Cao et al., 2016), their properties in the presence of stronger, potentially non-Gaussian noise, however, remain an area of active research. Standard techniques for covariance estimation quickly become computationally

infeasible in high-dimensional (Li et al., 2020) or irregular (Cederbaum et al., 2018) data settings and algorithmic innovations are required. Recently, Sarkar and Panaretos (2021) introduced promising neural network architectures for the efficient, nonparametric approximation of (multidimensional) covariance operators and their eigen-decomposition.

Several studies evaluated the consistency of covariance and FPCA estimators for incomplete curve settings. When incompleteness originates from a missing completely at random (MCAR) process and measurements are dense, established estimators for the mean, the covariance and for eigenfunctions and eigenvalues are consistent (Kraus, 2015). For the subject-specific functional principal component (FPC) scores, Kraus (2015) introduced a consistent estimator. His comparison to the PACE approach of Yao et al. (2005) indicates that the bias of comparable conditional methods for estimating the FPC scores is likely to be small.

Substantial bias can be caused by systematic missingness in the data. Liebl and Rameseder (2019) review certain violations of the MCAR assumption and motivate novel estimators for the mean and covariance structure for dense incomplete curve settings. While the classical estimators for the mean and covariance are consistent in regions of the domain with (virtually) no missingness, they are prone to (severe) bias the stronger the violation from the MCAR assumption and the fewer observations are available.

Estimation accuracy is also crucially affected by the coverage of the overall domain, especially so for estimating the covariance operator. Only if a sufficient number of observed curves overlap on the respective parts of their observed domains can the corresponding regions of the covariance surface be estimated reliably. For the setting of short observed domains ("functional fragments"), Delaigle et al. (2020), Descary and Panaretos (2019) and Zhang and Chen (2017) introduce conditions and approaches for consistently estimating (parts of) the covariance surface.

— Software implementations

Some general FPCA methods are implemented in R packages `fda` (Ramsay et al., 2020) and `refund` (Goldsmith et al., 2020). The multivariate FPCA approach of Happ et al. (2019) is implemented in package `MFPCA` (Happ-Kurz, 2020); the PACE algorithm of Yao

et al. (2005) in `fdapace` (Carroll et al., 2020). The methods outlined in Gertheiss et al. (2017) are available for the binary curves setting in `gfPCA` (Goldsmith, 2016), where the mixed regression in the two-step approach is estimated with package `gamm4` (Wood and Scheipl, 2020). Our accompanying package `registr` (Wrobel and Bauer, 2021) implements the Gaussian and binary curve GFPCA of Wrobel et al. (2019) as well as the two-step approach of Gertheiss et al. (2017) for various exponential family distributions.

3 Methods

As outlined, curves can have missing information at the beginning of their domain (i.e., *leading incompleteness*), at the end of their domain (*trailing incompleteness*), or both (*full incompleteness*). Our approach is able to handle all three types of incompleteness for curves observed on potentially irregular individual grids of evaluation points, without assuming Gaussianity of the observed data.

We first introduce our registration approach and the approach for generalized FPCA in full detail, and then present the main iterative algorithm to obtain a solution where the registered curves are well represented by a low-rank GFPCA basis. Potential identifiability issues and practical implications are discussed at the end of this section. Computational details are given in Appendix A1.

3.1 Registration for incomplete curves

We extend the likelihood-based framework for registering complete curves from exponential family distributions of Wrobel et al. (2019). In the registration step, the individual *chronological time domains* T_i^* are mapped onto the registered *internal time domain* T . This is achieved by estimating inverse warping functions h_i^{-1} that deform an unregistered curve $Y_i(t_i^*)$ toward a suitable template function $\mu_i(t)$ so that

$$\begin{aligned} \mathbb{E} [Y_i(h_i^{-1}(t_i^*)) | h_i^{-1}] &= \mu_i(t), \\ \text{with } h_i^{-1}(t_i^*) &= \Theta_h(t_i^*)\beta_i, \end{aligned} \tag{1}$$

with $Y_i(t)$ the registered curve. The inverse warping functions are represented through a B-spline basis with design matrix $\Theta_h \in \mathbb{R}_{D_i \times K_h}$, K_h basis functions and a corresponding coefficient vector β_i .

Given some distribution from the exponential family this yields the log-likelihood for curve i :

$$\ell(h_i^{-1}|y_i, \mu_i) = \log \left(\prod_{j=1}^{D_i} f_{i,j} [y_i(t_{i,j}^*)] \right), \quad (2)$$

with $f_{i,j}(\cdot)$ the corresponding density with expected value $\mu_i(h_i^{-1}(t_{i,j}^*))$ and observed vectors of function evaluations $y_i(t_{i,j}^*)$, $j = 1, \dots, D_i$. We impose working assumptions of mutual conditional independence across functions $[Y_i \perp Y_{i'}] | \mu_i, \mu_{i'}$ as well as within functions $[Y_i(t_{ij}) \perp Y_i(t_{ik})] | \mu_i$.

— Constrained optimization

Warping functions must follow certain constraints so that they yield reasonable transformations of the time domain. First, all warping functions have to be strictly increasing to preserve the temporal order of a curve’s measurements. Second, warping functions have to be domain-preserving with regard to the maximal domain of the underlying process. We ensure both by using a constrained optimization algorithm for the warping functions’ basis coefficients (see Appendix A1).

— Circumventing the constraint of fixed time intervals

If all curves are observed over an identical time interval, domain preservation requires that all warping functions map t_{\min}^* and t_{\max}^* to themselves so that they begin and end on the diagonal line. This assumption is made in most currently available registration procedures, based on an implicit assumption that the process of interest (e.g., the growth process of children) was observed from its very beginning up to its very end for all subjects. For incomplete curves, however, forcing observed and registered domain lengths to be identical is clearly unsuitable. We drop these hard constraints on the warping functions’ basis coefficients and allow warping functions to start and / or end at any point inside the overall time domain. To avoid large deformations of the time domain that are not strongly supported by the data, we penalize the total amount by which the registration changes the duration of the (observed) time domain. In a setting with full incompleteness, we use the

following penalized log-likelihood for the registration step:

$$\begin{aligned} \ell_{\text{pen}}(h_i^{-1}|y_i, \mu_i) &= \ell(h_i^{-1}|y_i, \mu_i) - \lambda \cdot n_i \cdot \text{pen}(h_i^{-1}), \\ \text{with } \text{pen}(h_i^{-1}) &= ([h_i^{-1}(t_{\max,i}^*) - h_i^{-1}(t_{\min,i}^*)] - [t_{\max,i}^* - t_{\min,i}^*])^2. \end{aligned} \quad (3)$$

For leading incompleteness with $h_i^{-1}(t_{\max,i}^*) = t_{\max,i}^* \forall i$, this simplifies to $\text{pen}(h_i^{-1}) = [h_i^{-1}(t_{\min,i}^*) - t_{\min,i}^*]^2$ and for trailing incompleteness with $h_i^{-1}(t_{\min,i}^*) = t_{\min,i}^* \forall i$ to $\text{pen}(h_i^{-1}) = [h_i^{-1}(t_{\max,i}^*) - t_{\max,i}^*]^2$. In other words, the penalty for one-sided incompleteness represents the squared distance of the respective endpoint of h_i^{-1} to the diagonal. The penalization parameter λ controls how much overall time dilation or compression the registration can perform and is scaled by the number of measurements n_i of curve i to ensure that the impact of the penalization relative to the likelihood is not affected by the number of measurement points per function. Details on the choice of λ are given in Section 3.4.

3.2 Generalized Functional PCA for incomplete curves

We adapt the *two-step approach* of Gertheiss et al. (2017) to estimate a low-rank GFPCA representation of the registered curves $Y_i(t) = Y_i(h_i^{-1}(t_i^*))$. Following Hall et al. (2008) and the groundwork of Yao et al. (2005), functional principal components (FPCs) are estimated using a marginal, semiparametric method based on assuming a latent Gaussian process $X_i(t)$ so that

$$\begin{aligned} \mathbb{E}[Y_i(t)] &= \mu_i(t) = g[X_i(t)], \\ X_i(t) &\approx \alpha(t) + \sum_{k=1}^K c_{i,k} \cdot \psi_k(t), \end{aligned} \quad (4)$$

where each observed $Y_i(t)$ corresponds to the transformation of the latent process $X_i(t)$ with some fixed response function $g(\cdot)$, and the latent process itself can be decomposed into a smooth global mean $\alpha(t)$, FPCs $\psi_k(t)$ with respective eigenvalues $\tau_k > 0$, and FPC scores $c_{i,k} \sim N(0, \tau_k)$. With known $\psi_k(t)$, model (4) is a generalized functional additive mixed model along the lines of Scheipl et al. (2016a) with a smooth conditional latent mean function in a P-spline representation, functional random effects in an FPC basis representation, and functional random effect scores $c_{i,k} \sim N(0, \tau_k)$. While the derivation of the covariance approximation below assumes that $X_i(t)$ shows only small variation around its

mean, stronger variation only has “a modest effect on the errors in individual predictions” (Hall et al., 2008, 4.2).

To derive the GFPCA solution, we first center the observed $Y_i(t)$ based on their marginal mean $\mu_Y(t) = \mathbb{E}[Y_i(t)]$, estimated through a simple smoother of all $(t_{ij}, Y_i(t_{ij}))$ -pairs via a generalized additive model (GAM, Fahrmeir et al., 2013) with response function $g(\cdot)$ and the appropriate exponential family for the response. The covariance of the latent process can then be approximated by

$$\widehat{\text{Cov}}[X_i(s), X_i(t)] \approx \frac{\hat{\sigma}_Y(s, t)}{g^{(1)}[\mu_X(s)] \cdot g^{(1)}[\mu_X(t)]}, \quad (5)$$

with $\sigma_Y(s, t) = \mathbb{E}[Y_{c,i}(s) \cdot Y_{c,i}(t)]$ based on the centered curves $Y_{c,i}(t)$, the marginal mean $\mu_X(t)$ estimated accordingly to $\mu_Y(t)$ and $g^{(1)}(\cdot)$ the first derivative of the response function. For given time points s_1 and s_2 , $\sigma_Y(s_1, s_2)$ is estimated as the mean of all pairwise products $y_{c,i}(s_1) \cdot y_{c,i}(s_2)$. The estimated surface $\hat{\sigma}_Y(s, t)$ is a smoothed version of $\sigma_Y(s, t)$ using a bivariate tensor product P-spline basis (Fahrmeir et al., 2013). Since the surface is expected to show some discontinuity along the diagonal this smoothing step is performed under exclusion of the diagonal elements (c.f. Yao et al., 2005). The FPCs $\psi_k(t)$ and their respective eigenvalues τ_k are then estimated from the spectral decomposition of $\widehat{\text{Cov}}[X_i(t), X_i(s)]$. Our approach deviates slightly from the method of Hall et al. (2008) it is based on: We mean-center the data before taking their crossproducts instead of subtracting the crossproduct of the estimated mean from the crossproducts of the data. In our experience, this yields smoother estimates of the covariance surface which are more amenable to a low-rank FPC representation.

3.3 Joint approach

We utilize the iterative algorithm of Wrobel et al. (2019) to combine the outlined approaches for registration and GFPCA. Our aims are twofold: (i) register all observed curves $Y_i(t_i^*)$ to suitable template functions and (ii) adequately represent the registered curves $Y_i(t) = Y_i(h_i^{-1}(t_i^*))$ through a low-rank GFPCA basis. We solve this problem by alternating the registration step (conditional on the current GFPCA representations $\mu_i(t)$) and the GFPCA step (conditional on the current estimates of the warping functions h_i^{-1}).

The initial registration step is performed with respect to a fixed common template function $\mu(t)^{[0]}$ which has to be set by the user. Subsequent iterations then use the low-rank GFPCA representations $\mu_i(t)$ as curve-specific template functions. Full details on the iterative estimation are given in Algorithm 1.

The number of FPCs in each iteration can be chosen based on the explained proportion of variance. We adapt this criterion to account for peculiarities of the covariance structure estimated with the two-step approach. Full details are discussed at the end of Section 3.4.

Algorithm 1 Joint Registration & GFPCA

Require: Observed curves $y_i(\mathbf{t}_i^*)$; starting template $\mu(t)^{[0]}$; explained share of variance κ_{var} of GFPCA solution; convergence tolerance Δ_h , iteration counter $q = 0$.

- 1: Initial registration of observed curves $y_i(\mathbf{t}_i^*)$ to global initial template $\mu(t)^{[0]}$ to initialize $\hat{h}_i^{-1}(t^*)^{[0]}$;
 - 2: **while** $\sum_{i=1}^N \left(\sum_{j=1}^{D_i} \left[\hat{h}_i^{-1}(t_{i,j}^*)^{[q]} - \hat{h}_i^{-1}(t_{i,j}^*)^{[q-1]} \right]^2 \right) > \Delta_h$ **do**
 - 3: $q \rightarrow q + 1$
 - 4: Update GFPCA using registered curves $y_i \left(\hat{h}_i^{-1}(\mathbf{t}_i^*)^{[q-1]} \right)$ (Section 3.2).
 - 5: Re-estimate GFPCA representations $\mu_i(t)^{[q]}$ based on the first $K^{[q]}$ FPCs that explain at least a share κ_{var} of the total variance (Model (4))
 - 6: Update warping function estimates $\hat{h}_i^{-1}(t^*)^{[q]}$ by re-registering observed curves $y_i(\mathbf{t}_i^*)$ to $\mu_i(t)^{[q]}$.
 - 7: **end while**
 - 8: Final GFPCA estimation based on the registered curves $y_i \left(\hat{h}_i^{-1}(\mathbf{t}_i^*)^{[q]} \right)$ to obtain GFPCA representations $\mu_i(t)$ based on the first K FPCs that explain at least share κ_{var} of the total variance.
-

3.4 Pitfalls and Practical Considerations

— Identifiability

A common issue in the separation of amplitude and phase variation is that disentangling the two types of variation is an ill-posed problem in most realistic settings. Structured variability in the curves can almost always be attributed to either warpings of the time

domain or superpositions of principal components, or any combination of the two. Both Chakraborty and Panaretos (2017) and Wagner and Kneip (2019) have shown that the general registration problem has a unique solution only if the amplitude variation is of rank 1, i.e. for FPC rank $K = 1$. In practice, this non-identifiability can be removed by introducing suitable inductive biases for estimates of the warping and template functions through priors, penalties and/or limiting the expressivity of model components, e.g. by choosing low-rank basis representations. We assess the severity of this identifiability problem for our method in a simulation study in Section 4. Note that the low-rank basis representations of the warping functions we employ also seem to successfully avoid the “pinching” problem (see e.g. Ramsay and Li, 1998, 4.2).

— **Choice of the template function**

As outlined above, the template function $\mu(t)^{[0]}$ for the initial registration step in the joint estimation has to be set by the user. The choice should be based on subject knowledge and can be crucial for obtaining reasonable results (compare Appendix A7) and quick convergence in subsequent iterations.

— **Choice of the penalization parameter λ**

Our registration approach controls the overall amount of compression or dilation through the penalization parameter λ . The choice of λ should be based on substantive knowledge so that estimated warping functions represent realistic accelerations and/or decelerations of the observed processes.

— **Choice of the number of FPCs**

The number of FPCs can be chosen based on the explained share of variance of the low-dimensional FPC basis. In this regard, the two-step approach faces two issues: First, since the spectral decomposition is applied to a smoothed covariance surface and not the raw covariance of the data itself, the “explained” share of variance is relative to this “structured” part of the total observed variance. Second, based on our practical experience, spectral decompositions of covariance surfaces often yield a large number of subordinate FPCs which each explain only a very small amount of overall variation, but jointly explain a relevant share. As we show in Appendix A6, it can be argued that these subordinate FPCs often

represent phase variation rather than amplitude variation.

We deliberately avoid including such subordinate FPCs in the FPCA solution since the FPCs in the joint approach should only represent the main amplitude variation. Our goal is to find suitable template functions to register against which don't include modes of phase variation, i.e., the template functions do not need to represent each individual registered curve with high fidelity. Accordingly, we suggest a two-fold criterion for choosing the number of FPCs based on our two-step approach: Choose as many FPCs as are needed to explain a large portion (90%, by default) of the overall structured variation. However, do not include such FPCs in the final solution that account for very little variation (less than 2%, by default). In this way, we define a low-rank FPCA representation for the template functions which might explain less than 90% of the overall variation but does not include a multitude of subordinate modes of (phase) variation.

4 Simulation Study

To assess the performance of our method and compare it to other established approaches we perform a simulation study on both Gaussian and Gamma data, motivated by our seismic application. We focus on the comparison of approaches that jointly perform registration and FPCA and assess (i) their ability to recover de-noised underlying curves, (ii) their performance in disentangling and estimating the underlying amplitude and phase variation, and (iii) their computational efficiency.

We compare our proposal (called “FGAMM” in the following) – combining two-step FPCA with our (in)complete curve registration – with the earlier approach of Wrobel et al. (2019) (“varEM”) – using an identical registration approach combined with a variational EM-based FPCA – and the joint SRVF approach of Tucker (2014) (Algorithm 4.1, “SRVF”) which combines the SRVF registration of Srivastava et al. (2011) with the vertical fPCA introduced in Tucker et al. (2013). The latter approach is only applied to complete curve settings since the software implementation available at the time of writing (Tucker, 2020, R-package `fdasrvf`) is not able to handle incomplete curves.

4.1 Simulation design

In each simulation setting, we first simulate $N = 100$ complete curves on a regular time grid on $[0, 1]$ with length $D_i = 50 \forall i$ from model (4) with FPC rank $K \in \{1, 3, 4\}$, with

- mean function $\alpha(t)$ a Gaussian density function with $\mu = 0.45$ and $\sigma = 0.2$,
- eigenfunctions $\psi_k(t)$ as the $(k + 1)$ th orthonormal polynomial on $[0, 1]$,
- mutually independent FPC scores $c_{i,k} \sim N(0, \tau_k)$ and $\boldsymbol{\tau} = 1$ for $K = 1$, $\boldsymbol{\tau} = (0.7, 0.25, 0.05)$ for $K = 3$, $\boldsymbol{\tau} = (0.4, 0.3, 0.2, 0.1)$ for $K = 4$,
- Gaussian setting: $Y_i(t_j) \sim N(X_i(t_j), \sigma^2 = 0.03)$,
- Gamma setting: $Y_i(t_j) \sim \Gamma(k = 5, \theta = \frac{1}{5} \exp(X_i(t_j)))$,

with $X_i(t_j) = \alpha(t) + \sum^K \psi_k(t)c_{i,k}$ the simulated (latent) process.

Warping functions are simulated utilizing a B-spline basis using cubic splines and three degrees of freedom. Their basis coefficients are drawn from a uniform distribution over $[0, 1]$ and cumulatively summed up to ensure monotony. Three settings of (in)completeness are analyzed: Complete curves, weak incompleteness and strong incompleteness. The latter two settings only comprise trailing incompleteness. Weak incompleteness and strong incompleteness are simulated by randomly drawing a cut-off time from a uniform distribution over the last 40% and 70% of the time domain, respectively.

Regarding the correlation structure between the extents of (i) amplitude variation, (ii) phase variation and (iii) incompleteness we analyze three different settings. In the first, the three dimensions are mutually uncorrelated. The second setting comprises a strong negative correlation between amplitude and phase variation, shifting the peaks of curves with larger amplitudes towards the beginning of the domain. The third setting comprises a stronger positive correlation between amplitude and the amount of incompleteness, resulting in stronger incompleteness for curves with lower amplitudes.

Visualizations of the simulated data can be found in Appendix A3.1. For the methods FGAMM and varEM, we use eight and four basis functions for the estimation of the mean curve and the inverse warping functions, respectively. In the Gaussian setting, the

penalization parameter is set to $\lambda = 0.025$. In the Gamma setting, it is set to 1 and 0.5 for FGAMM (assuming a Gamma distribution) and varEM (assuming a Gaussian distribution), respectively. The observed overall mean curve is used as the initial template function. In the FGAMM approach, the covariance surface is smoothed with ten marginal P-spline basis functions. Since the implementation of the SRVF approach relies on the curves being observed on a regular grid, the simulated curves are linearly interpolated onto a regular grid. We perform 100 replications for each simulation setting and method. The following results only cover the simulation settings without correlation between phase, amplitude and incompleteness. Unless noted otherwise, the results for the other simulation settings are structurally similar (see Appendices A3.2 and A3.3).

— **Adaptive estimation of the number of FPCs**

The number of estimated FPCs was pre-set to the respective true simulated amplitude rank. While our method includes adaptive, data-based estimation of the number of FPCs (see Algorithm 1), we did not pursue this approach here since this would jeopardize our ability to differentiate (i) its ability to recover FPCs and their scores accurately and (ii) its ability to select a suitable number of FPCs based on the data. Additional results based on the more realistic use-case with adaptive estimation of the FPCs are given in Appendices A3.4 and A3.5. The methods’ performances on the Gaussian simulation settings with adaptively estimated FPC rank K are structurally similar to the ones with pre-specified rank. In the Gamma settings, while this is the case for the estimated phase components, all methods struggle to recover the correct number of FPCs and specifically the varEM approach performs worse in terms of the estimation of amplitude variation.

4.2 Results

— **Performance metrics**

We base our method comparisons in Figures 3 and 4 on different performance metrics, most based on the mean (integrated) squared error (MISE, MSE) for functional and scalar estimates, respectively. Overall performance is quantified using the difference between the simulated individual mean structures (before adding random noise) and the respective rep-

representations based on the final FPCA solution (measure MISE_y). This metric indicates how well the complete structured variation, i.e, the combined phase and amplitude variation, of the observed data is recovered. The performance regarding the separation and estimation of amplitude and phase variation is quantified by (i) comparing the spans of the true and estimated FPC bases with a measure introduced by Larsson and Villani (2001) and adapted by Scheipl et al. (2016b) (amplitude variation, LV_ψ) and by (ii) comparing the true and estimated warping functions (phase variation, MISE_h). Following Scheipl et al. (2016b), the measure LV_ψ quantifies the overlap of the spans of two matrices $\mathbf{A} \in \mathbb{R}^{n \times p_A}$ and $\mathbf{B} \in \mathbb{R}^{n \times p_B}$, $n > p_A, p_B$:

$$\text{LV}_\psi(\mathbf{A}, \mathbf{B}) = \frac{1}{p_A} \cdot \text{trace}(\mathbf{V}_B^T \mathbf{V}_A \mathbf{V}_A^T \mathbf{V}_B),$$

with \mathbf{V}_Z , $Z \in \{A, B\}$, a matrix of the left singular vectors of matrix \mathbf{Z} . We scale the measure by the dimension of the true FPC basis p_A to obtain a codomain of $[0, 1]$ where value 1 encodes perfect representation of the true amplitude variation space and 0 represents completely orthogonal spans. In accordance with the other performance measures we report $1 - \text{LV}_\psi$ so that smaller values encode better performance. Note that LV_ψ cannot be computed for the SRVF approach since that method is based on an FPCA of the SRVF transforms of the original functions and does not yield orthonormal eigenfunctions in the original function space. Finally, we compute the estimation performance of the overall amount of time dilation or compression by comparing the true and estimated domain lengths of the registered curves (MSE_d).

— Results Gaussian settings

The results for the Gaussian settings are visualized in Figure 3. While methods varEM and FGAMM do a good job in representing the underlying structured variation (MISE_y) and in estimating both warping functions (MISE_h) and original domain lengths (MSE_d), amplitude variation (LV_ψ) is only estimated with higher accuracy for amplitude rank 1. Both FPCs and warping functions are estimated more accurately if amplitude variation has smaller rank.

Comparing the methods and focusing only on the complete curve settings (left panels) for which it is applicable, the joint SRVF approach performs consistently worse than the

other two approaches. For $MISE_y$ and $MISE_h$ the median performance of FGAMM for amplitude rank 2–3 is better by 89% and 79% compared to SRVF, respectively. The varEM approach performs slightly better than FGAMM for the complete curve settings in terms of representing the overall variation, and slightly worse in terms of recovering the space of amplitude variation. Regarding the incomplete curve settings, the incomplete curve approaches perform consistently best with respect to MSE_d and $MISE_y$. The estimated curve representations contain a much higher share of the originally observed variation than is represented by methods with assumed completeness. While the incomplete curve approaches mostly perform better in terms of phase variation ($MISE_h$ and MSE_d), this is not consistently the case for the estimation of amplitude variation (LV_ψ). In summary, among the evaluated incomplete curve methods, varEM performs somewhat better than FGAMM, especially for representing the observed variation. We do not observe a large drop in estimation performance between the settings with weak and strong incompleteness.

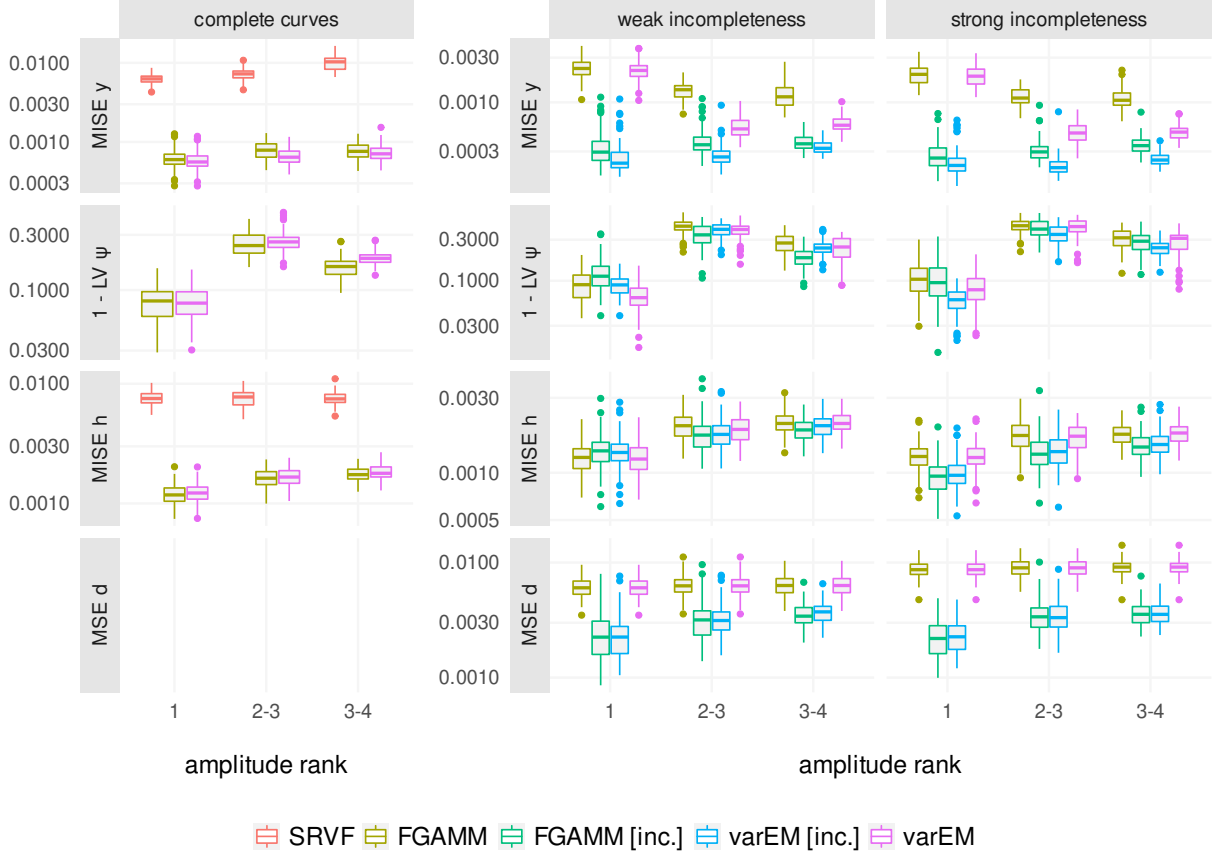


Figure 3: Results for the simulation setting with Gaussian data and mutually uncorrelated amplitude, phase and amount of incompleteness. All y scales are \log_{10} transformed.

— Results Gamma settings

For the Gamma settings, the varEM and SRVF approaches fall back on a misspecified Gaussian or "least squares" approach since neither are implemented for Gamma data. FGAMM utilizes the appropriate Gamma likelihood for both registration and GFPCA steps. The results are displayed in Figure 4. All in all, for the setting without correlation between amplitude, phase and incompleteness, the performance with regard to $MISE_h$ and MSE_d is similar to the Gaussian case. All methods show consistently worse performance than in the Gaussian setting in terms of $MISE_y$ and LV_ψ , also for small amplitude ranks.

On complete data, the SRVF approach again performs worst in terms overall representation and warping function estimation, with the FGAMM median performance for

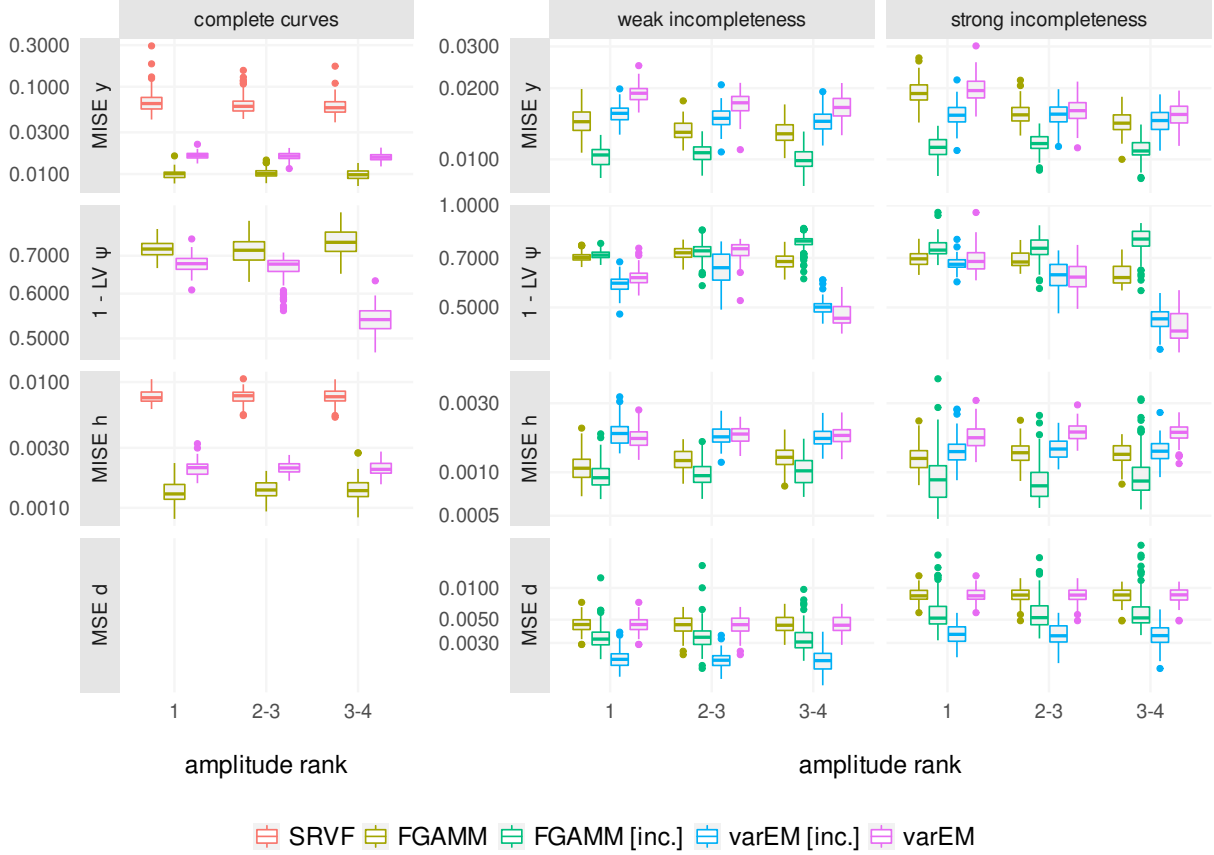


Figure 4: Results for the simulation setting with Gamma data and uncorrelated amplitude, phase and amount of incompleteness. All y scales are \log_{10} transformed.

amplitude rank 2–3 being better by 83% and 82%, respectively. Regarding the estimation of the overall representation and the warping functions, the (incomplete) FGAMM approach assuming the Gamma structure performs consistently better than varEM. However, FGAMM performs worse in recovering the FPC space, especially for the largest amplitude rank. For the estimation of the amplitude structure and the domain lengths, varEM leads to consistently better results. Comparing these results to the settings with weak and strong incompleteness, the latter only show a structurally worse estimation performance for MSE_d .

4.3 Runtime analysis

We evaluate the efficiency of the approaches on one simulation setting with a Gaussian structure, amplitude rank 2–3 and complete curves. Only FGAMM is additionally applied to the respective setting with Gamma data. The median runtimes of each method, based on 20 runs, are visualized in Figure 5.

For the comparison, methods FGAMM and varEM (“varEM 2.1”) are based on function `register_fpca` in version 2.1.5 of the `registr` package, which uses methods from packages `gamm4` (Wood and Scheipl, 2020) (v0.2.7) and `lme4` (Bates et al., 2015) (v1.1.26). These methods are compared to the old version of `registr` (v1.0.0, based on `gamm4` v0.2.6 and `lme4` v1.1.23), which does not contain the algorithmic improvements outlined in Appendix A1. We also compare our methods to function `align_fPCA` of package `fdasrvf` (Tucker, 2020) (v1.9.4) which implements the joint SRVF approach. All methods except version 1.0 of package `registr` (“varEM 1.0”) were run in parallel mode using ten cores.

— Main findings

As can be seen in Figure 5, the optimized algorithm in varEM 2.1 is clearly the most efficient method. For the setting with 50 measurements per curve and 3 000 curves (“ $D_i = 50, N = 3000$ ”) varEM 2.1 (runtime 23 seconds) is on average 86% faster than varEM 1.0 (159 seconds). The estimation of FGAMM is computationally much more expensive. For the setting “ $D_i = 50, N = 3000$ ” it takes about 14 min, i.e., 37 times longer than varEM 2.1. Also, the runtime of FGAMM scales quadratically in both the number of curves and the number of measurements per curve. The efficiency of the SRVF approach lies between the other methods for smaller samples. However, it becomes computationally demanding for densely observed datasets with higher numbers of measurements per curve.

5 Application

5.1 Berkeley growth study

We compare FGAMM and varEM results on the well-known Berkeley growth data with simulated strong full incompleteness as outlined in Section 1 and visualized in Appendix A4.1.

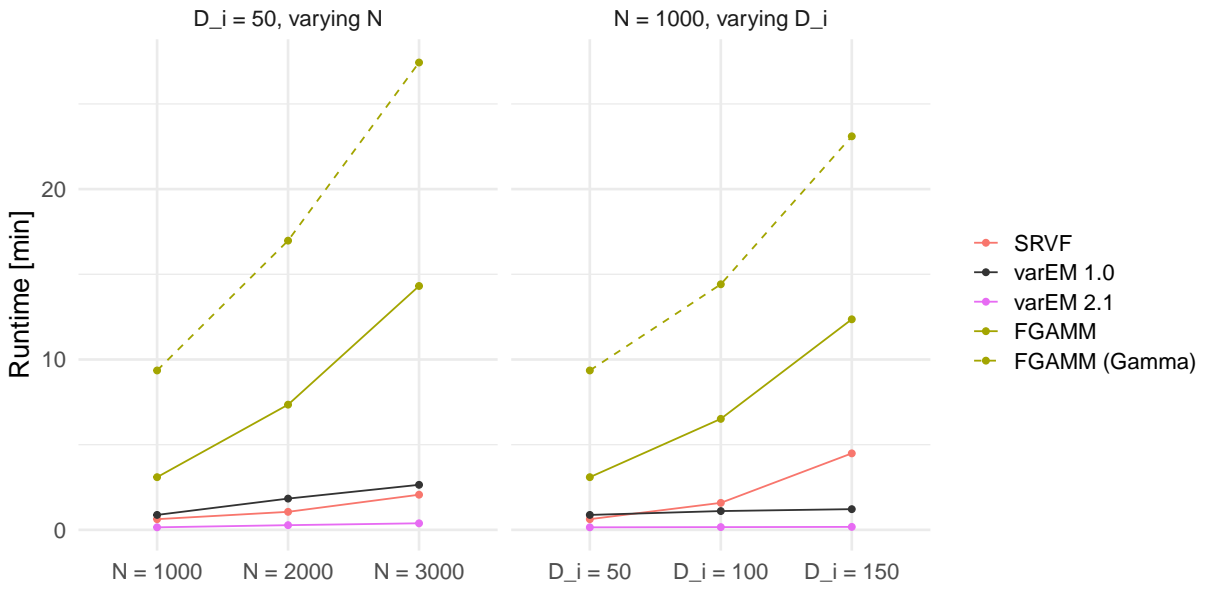


Figure 5: Median runtimes for one setting of the simulation study with amplitude rank 2-3 and no incompleteness, based on 20 runs for each parameter combination. For the analysis, we vary the number of curves N and the number of measurements per curve D_i . Dashed curves are runtimes for FGAMM (Gamma).

That is, we randomly remove both leading and trailing segments of the curves, with starting points and endpoints drawn at random in the first quarter and the last half of the time domain, respectively. Both methods are then applied with and without the assumption of completely observed curves, using a Gaussian likelihood and the same hyperparameters as used for the simulation study. The number of FPCs to be used in each iteration of the joint registration and FPCA algorithm was estimated adaptively, based on the criterion outlined at the end of Section 3.

While the FGAMM approach chose 5 (assuming completeness) and 4 (incomplete) FPCs, the varEM method chose 7 and 6 FPCs, respectively. In the comparison in Figure 6, we focus on the first two FPCs estimated by each method. Results in full detail are given in Appendix A4.2. Appendix A4.3 shows how the results of the incomplete curve FGAMM approach changes when different values for the penalization parameter λ are used.

While the first two FPCs estimated by the methods with assumed incompleteness show some differences, they represent similar main modes of amplitude variation. The first FPC mainly represents variation at the very beginning of the domain along with the information that the peak in growth in adolescent age appears earlier on if the growth rate in the very first year was stronger. The second FPC represents the information that if the initial growth rate was higher, the peak in adolescent age is more attenuated.

These first two FPCs as estimated by the incomplete curve approaches differ from the first FPCs estimated with assumed completeness. This is mainly due to the fact that the “completeness-assumed” approaches are not able to adequately align the structures observed in the last third of the domain (c.f. top row of Figure 6). In this data setting, the incomplete curve approaches are clearly better able to recover the underlying phase variation in the curves. In terms of computation time, both FGAMM variants and the incomplete varEM take about a minute, while varEM assuming completeness takes almost 2 minutes.

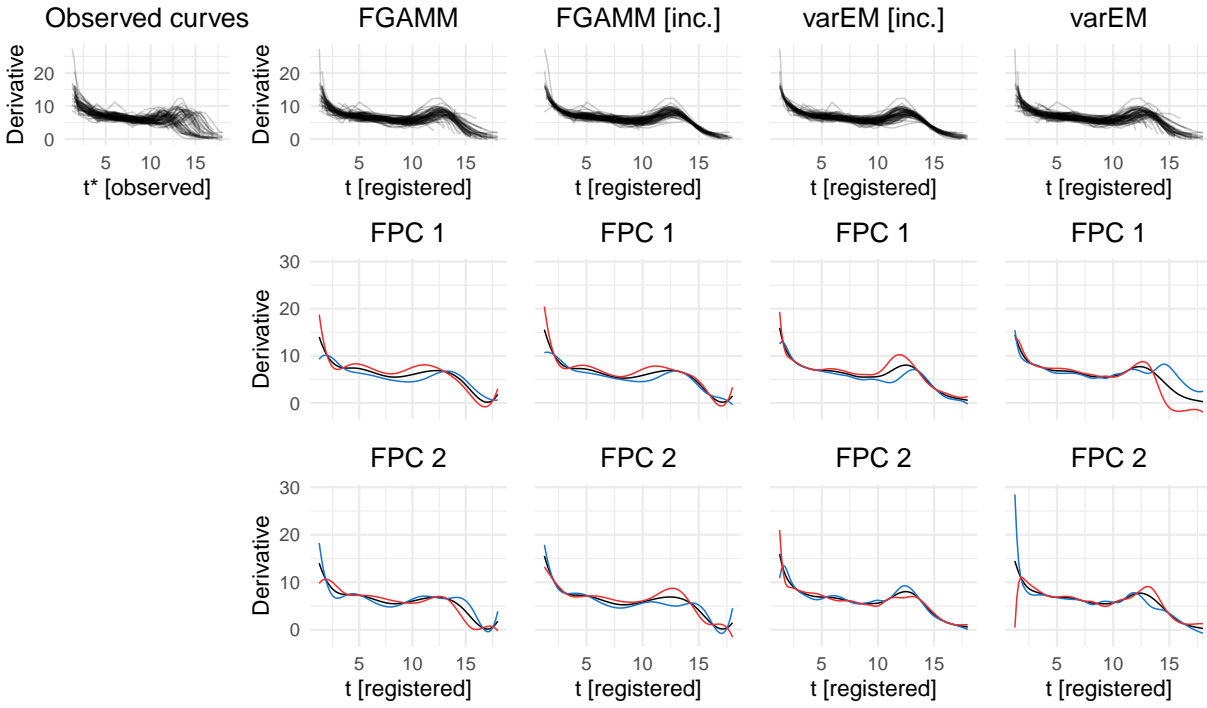


Figure 6: Observed curves with simulated incompleteness (top left pane), registered curves (top row) and the first two estimated FPCs based on the different approaches. The FPCs $\psi_k(t)$ are visualized by the overall mean curve (solid line) plus (blue line) and minus (red line) $2 \cdot \sqrt{\hat{\tau}_k} \cdot \psi_k(t)$, with $\sqrt{\hat{\tau}_k}$ the standard deviation of the estimated scores for the k 'th FPC.

5.2 Seismic ground motion propagation

We analyze a subset of seismological interest of the seismic data outlined in Section 1, comprising 2 484 curves from various earthquakes simulated with different physical parameters. Sepcifically, we use data from simulated quakes characterized by (i) a sedimentary subsurface structure amplifying ground shaking, (ii) a geologically well-oriented direction of the tectonic background stress between 27° and 35° , and (iii) the friction parameter of critical linear slip weakening distance between 1.1m and 1.5m. We also restrict the data to those seismograms most relevant for seismic hazard assessment, which (i) lie in forward directivity direction (between cardinal directions 280° and 342°) to focus on wave propagations to the northwest in the direction of the main rupture pulse, and (ii) with a hypocentral distance shorter than 35km. Previous analyses show that the ground velocity curves we study are primarily shaped by the hypocentral distance of the measurement station and the *dynamic coefficient of friction* which resembles the frictional resistance of the geological fault during earthquake propagation (Bauer et al., 2017). For our analysis, we focus on how these two parameters and the topography of the evaluated region are associated with phase and amplitude variation.

As shown in Figure 2, all curves are pre-processed by cutting off any leading zero measurements below 0.01, leading to the observed time domain t_0^* which – being the *time since the first relevant absolute ground velocity measurement* – begins with the arrival time of seismic P-waves and comprises trailing incompleteness only towards the end of the domain after $t_0^* = 23.5$ seconds. Since this induces a MAR structure, where short observed domain lengths are caused by higher hypocentral distances (causing later P-wave arrival times and smaller amplitudes), the results towards the end of the domain must be interpreted with great care.

We apply the FGAMM approach assuming a Gamma structure and trailing incompleteness, and using a similar parametrization as in the simulation study. The mean curve of all observed curves was used as the template function for the initial registration step. We use a penalization parameter of $\lambda = 0.004$ to discourage extreme distortions of the time domain. Estimation of the joint approach took ten joint iterations and a runtime of 3:31h using

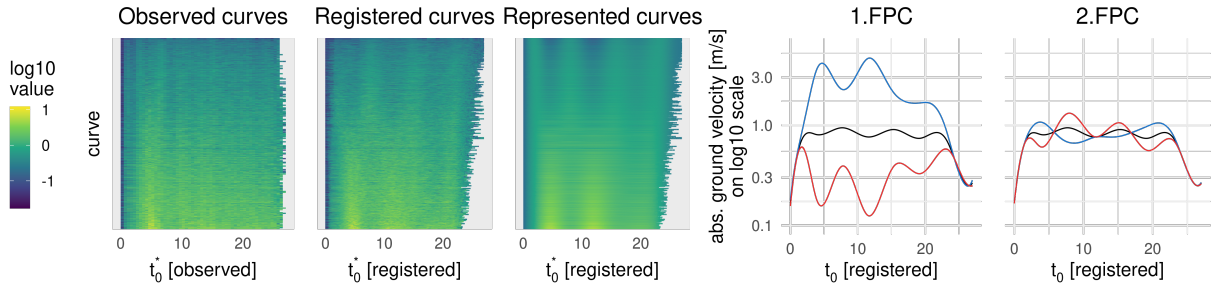


Figure 7: Lasagna plots of observed and registered curves and of the curves as represented by the final GFPCA solution based on the FGAMM approach, on log10 scale (left pane). Curves are sorted by their maximum observed value. The FPCs $\psi_k(t)$ are visualized by the overall mean curve (black line) plus (blue line) and minus (red line) $2 \cdot \sqrt{\hat{\tau}_k} \cdot \psi_k(t)$, with $\sqrt{\hat{\tau}_k}$ the standard deviation of the estimated scores for the k 'th FPC (right pane).

a parallelized call for the registration steps with 5 cores. Two FPCs were chosen based on the selection criterion outlined in Section 3 when aiming to explain 95% of amplitude variation.

The two estimated FPCs along with the observed, registered and represented curves are visualized in Figure 7. The full estimated warping functions are shown in Appendix A5.1. The first FPC as the main mode of amplitude variation represents the overall magnitude of the ground velocities, shaped by two salient peaks that resemble the shaking caused by surface wave phase arrivals. The second FPC represents a subsequent mode of variation and mainly shapes how pronounced the initial peak is.

The associations of phase and amplitude variation with the hypocentral distance and the dynamic coefficient of friction are visualized in Figure 8. Amplitude variation shows a very pronounced association structure with both parameters. Focusing on the first FPC, ground velocities are overall stronger the closer the measurement was taken to the hypocenter and the smaller the dynamic friction. The strongest ground motion is observed at hypocentral distances between 20 and 25km, caused by the nonlinear interaction of rupture propagation and the radiated seismic wavefield with topography and the subsurface structure. We find that in this region source effects (rupture directivity) and seismic wave path effects (surface

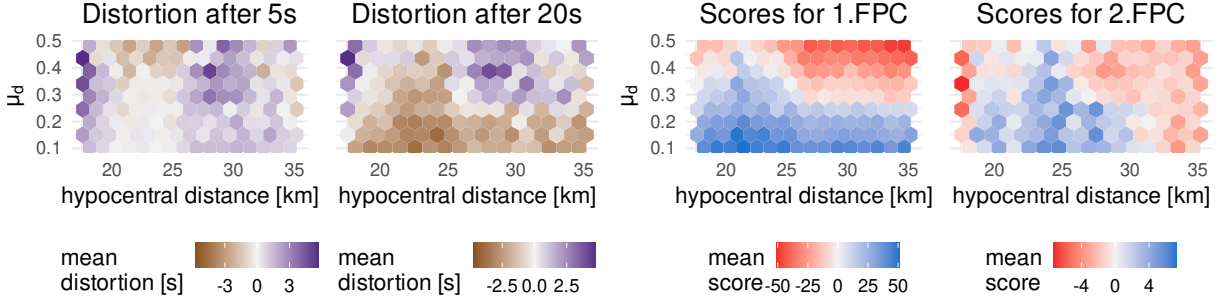


Figure 8: Estimated phase and amplitude variation conditional on the hypocentral distance of the virtual seismometer and the dynamic coefficient of friction μ_d of the simulation. Phase variation and amplitude variation are shown by displaying the mean of the overall time distortion after 5 and 20 seconds (left pane, with positive and negative values representing time dilation and compression, respectively) and of the curves' mean scores for the FPCs shown in Figure 7, respectively.

waves) unleash the most energy. The second FPC's scores show a somewhat similar association structure but are more strongly shaped by the hypocentral distance. The highest scores were estimated at around 25km of distance, representing the most pronounced initial peak structure, especially in simulations with low dynamic friction values.

Phase variation is also strongly associated with both evaluated parameters. The estimated time distortions at time t given by $\hat{h}_i^{-1}(t) - t$ for $t \in \{5, 20\}$ show somewhat similar patterns to the association structures of the FPC scores. This corroborates the structure displayed in Figure 2 which indicates a strong coupling between amplitude and phase variation since the initial peak is generally observed later for smaller overall observed ground velocities (an effect known in seismology as geometrical spreading). Stronger time distortion of the initial five seconds was mostly estimated for medium-to-large friction values, which are accompanied by smaller ground velocities. While these initial five seconds for curves observed between 20 and 25km of hypocentral distance (shaped by a more pronounced structure of the initial peak around $t_0 = 5$, see Figure 7) were mainly compressed, for curves closer to and farther away from the hypocenter (shaped by a less salient initial peak around $t_0 = 2$) they were mainly dilated. The time distortion of the initial 20 sec-

onds shows a very similar structure to the scores for the first FPC. For curves with higher ground velocities, these initial 20 seconds are mainly compressed, and mainly dilated for lower ground velocities. Finally, the estimated inverse warping functions more often tend to more extreme distortions for higher hypocentral distance and higher dynamic friction values (see Appendix A5, Figure 20). This is due to curves under these conditions showing very small ground velocities with a less salient structure that is hard to align to the estimated template functions.

As expected due to the dominant effects of source directivity and surface waves in the evaluated region around the hypocenter, no structural association of amplitude or phase variation with the local topography was detected (see Appendix A5.2). The obtained results are geophysically plausible and in line with previous analyses of the seismic experiments (Bauer et al., 2017).

6 Discussion

Incomplete data are very common in longitudinal settings but remain under-discussed in many fields of functional data analysis. Our likelihood-based approach for joint registration and generalized FPCA allows for analyzing curves with leading, trailing or full incompleteness in the presence of substantial phase variation and is able to handle non-Gaussian data. All methods are implemented in the open-source R package `registr`.

Our simulation study results indicate that accounting for incompleteness improves the performance in different data settings. While the FGAMM approach shows some bias in the estimation of the underlying FPC structure in the Gamma settings, its substantially better estimation of the warping functions leads to improved overall performance in terms of the representation of the joint phase and amplitude variation structure of the individual curves. Stronger incompleteness does not seem to structurally harm the overall performance. Applications to incomplete Berkeley growth curves and a seismic data setting showcase the practical utility of our new approach.

— Comparison to SRVF-based approaches

In contrast to methods based on the SRVF framework, we do not utilize the warping-

invariant Fisher-Rao metric. Instead, our flexible penalized likelihood-based approach allows for representing more complex structures of variation in diverse non-Gaussian data situations and is backed by robust optimization algorithms. While SRVF approaches rely on the availability of functional derivatives evaluated on a common, regular grid and may struggle in the presence of stronger (non-Gaussian) noise, this is generally not the case for our method. We utilize a low-dimensional B-spline basis for the inverse warping functions. In our applications, this seemed sufficient to avoid the pinching problem. Extreme time distortions were only estimated for few seismic curve outliers without a pronounced shape.

— Covariance estimation

One central topic for future research on GFPCA is a thorough evaluation of the consistency and robustness of different covariance estimators. This comprises questions like at what point in the estimation procedure smoothing and centering (of the raw curves or the final covariance surface) should be performed to obtain the best estimator. Covariance estimators should be evaluated for common practical data settings entailing relevant non-Gaussian noise in combination with small numbers of curves and measurements per curve and different levels of their respective density over the domain.

— Computational efficiency

A practical constraint for the application of the evaluated methods remains their computational efficiency in large-scale data settings. In this regard, a promising strain of research are recently proposed neural network based frameworks like Nunez et al. (2021) and Chen and Srivastava (2021) for registration and Sarkar and Panaretos (2021) for covariance estimation.

References

- Bates, D., Mächler, M., Bolker, B., and Walker, S. (2015), “Fitting Linear Mixed-Effects Models Using lme4,” *Journal of Statistical Software*, 67, 1–48.
- Bates, D., Mullen, K. M., Nash, J. C., and Varadhan, R. (2014), *minqa: Derivative-free optimization algorithms by quadratic approximation*, R package version 1.2.4.

- Bauer, A. (2021), “bauer-alex/IncFunDatRegistration_supp: Full code and data supplement,” .
- Bauer, A., Scheipl, F., Küchenhoff, H., and Gabriel, A.-A. (2017), “Modeling spatio-temporal earthquake dynamics using generalized functional additive regressions,” in *International Workshop on Statistical Modelling 2017*.
- Bauer, A., Scheipl, F., Küchenhoff, H.— (2018), “An introduction to semiparametric function-on-scalar regression,” *Statistical Modelling*, 18, 346–364.
- Bryner, D., and Srivastava, A. (2021), “Shape Analysis of Functional Data with Elastic Partial Matching,” *arXiv preprint arXiv:2105.08604*.
- Cao, G., Wang, L., Li, Y., and Yang, L. (2016), “Oracle-efficient confidence envelopes for covariance functions in dense functional data,” *Statistica Sinica*, 26, 359–383.
- Carroll, C., Gajardo, A., Chen, Y., Dai, X., Fan, J., Hadjipantelis, P. Z., Han, K., Ji, H., Mueller, H.-G., and Wang, J.-L. (2020), *fdapace: Functional Data Analysis and Empirical Dynamics*, R package version 0.5.5.
- Cederbaum, J., Scheipl, F., and Greven, S. (2018), “Fast symmetric additive covariance smoothing,” *Computational Statistics & Data Analysis*, 120, 25–41.
- Chakraborty, A., and Panaretos, V. M. (2017), “Functional Registration and Local Variations: Identifiability, Rank, and Tuning,” *arXiv preprint arXiv:1702.03556*.
- Chen, C., and Srivastava, A. (2021), “SrvfRegNet: Elastic Function Registration Using Deep Neural Networks,” in *Proceedings of the IEEE/CVF Conference on Computer Vision and Pattern Recognition*, pp. 4462–4471.
- Cheng, W., Dryden, I. L., Huang, X. et al. (2016), “Bayesian registration of functions and curves,” *Bayesian Analysis*, 11, 447–475.
- Claeskens, G., Silverman, B. W., and Slaets, L. (2010), “A multiresolution approach to time warping achieved by a Bayesian prior–posterior transfer fitting strategy,” *Journal of the Royal Statistical Society: Series B (Statistical Methodology)*, 72, 673–694.

- Delaigle, A., Hall, P., Huang, W., and Kneip, A. (2020), “Estimating the covariance of fragmented and other related types of functional data,” *Journal of the American Statistical Association*, 1–19.
- Descary, M.-H., and Panaretos, V. M. (2019), “Recovering covariance from functional fragments,” *Biometrika*, 106, 145–160.
- Fahrmeir, L., Kneib, T., Lang, S., and Marx, B. (2013), *Regression: models, methods and applications*, Springer Science & Business Media.
- Gertheiss, J., Goldsmith, J., and Staicu, A.-M. (2017), “A note on modeling sparse exponential-family functional response curves,” *Computational statistics & data analysis*, 105, 46–52.
- Giorgino, T. (2009), “Computing and Visualizing Dynamic Time Warping Alignments in R: The dtw Package,” *Journal of Statistical Software*, 31, 1–24.
- Goldsmith, J. (2016), *gfpc: Generalized Functional Principal Components Analysis*, R package version 1.1.0. URL <https://github.com/jeff-goldsmith/gfpc>.
- Goldsmith, J., Scheipl, F., Huang, L., Wrobel, J., Di, C., Gellar, J., Harezlak, J., McLean, M. W., Swihart, B., Xiao, L., Crainiceanu, C., and Reiss, P. T. (2020), *refund: Regression with Functional Data*, R package version 0.1-23.
- Goldsmith, J., Zipunnikov, V., and Schrack, J. (2015), “Generalized multilevel function-on-scalar regression and principal component analysis,” *Biometrics*, 71, 344–353.
- Guo, X., Kurtek, S., and Bharath, K. (2020), “Variograms for spatial functional data with phase variation,” *arXiv preprint arXiv:2010.09578*.
- Hadjipantelis, P. Z., Aston, J. A., Müller, H.-G., and Evans, J. P. (2015), “Unifying amplitude and phase analysis: A compositional data approach to functional multivariate mixed-effects modeling of Mandarin Chinese,” *Journal of the American Statistical Association*, 110, 545–559.

- Hall, P., Müller, H.-G., and Yao, F. (2008), “Modelling sparse generalized longitudinal observations with latent Gaussian processes,” *Journal of the Royal Statistical Society: Series B (Statistical Methodology)*, 70, 703–723.
- Happ, C., Scheipl, F., Gabriel, A.-A., and Greven, S. (2019), “A general framework for multivariate functional principal component analysis of amplitude and phase variation,” *Stat*, 8, e220.
- Happ-Kurz, C. (2020), *MFPCA: Multivariate Functional Principal Component Analysis for Data Observed on Different Dimensional Domains*, R package version 1.3-6.
- Huang, H., Li, Y., and Guan, Y. (2014), “Joint modeling and clustering paired generalized longitudinal trajectories with application to cocaine abuse treatment data,” *Journal of the American Statistical Association*, 109, 1412–1424.
- James, G. M., Hastie, T. J., and Sugar, C. A. (2000), “Principal component models for sparse functional data,” *Biometrika*, 87, 587–602.
- Johnson, S. G. (2020), *The NLopt nonlinear-optimization package*, uRL <https://github.com/stevengj/nlopt>.
- Kneip, A., and Gasser, T. (1992), “Statistical tools to analyze data representing a sample of curves,” *The Annals of Statistics*, 1266–1305.
- Kneip, A., and Ramsay, J. O. (2008), “Combining registration and fitting for functional models,” *Journal of the American Statistical Association*, 103, 1155–1165.
- Kraus, D. (2015), “Components and completion of partially observed functional data,” *Journal of the Royal Statistical Society: Series B: Statistical Methodology*, 777–801.
- Kurtek, S. (2017), “A geometric approach to pairwise Bayesian alignment of functional data using importance sampling,” *Electronic Journal of Statistics*, 11, 502–531.
- Larsson, R., and Villani, M. (2001), “A distance measure between cointegration spaces,” *Economics Letters*, 70, 21–27.

- Learned-Miller, E. G. (2005), “Data driven image models through continuous joint alignment,” *IEEE Transactions on Pattern Analysis and Machine Intelligence*, 28, 236–250.
- Lee, S., and Jung, S. (2016), “Combined analysis of amplitude and phase variations in functional data,” *arXiv preprint arXiv:1603.01775*.
- Li, C., Xiao, L., and Luo, S. (2020), “Fast covariance estimation for multivariate sparse functional data,” *Stat*, 9, e245.
- Li, Y., and Guan, Y. (2014), “Functional principal component analysis of spatiotemporal point processes with applications in disease surveillance,” *Journal of the American Statistical Association*, 109, 1205–1215.
- Liebl, D., and Rameseder, S. (2019), “Partially observed functional data: The case of systematically missing parts,” *Computational Statistics & Data Analysis*, 131, 104–115.
- Lu, Y., Herbei, R., and Kurtek, S. (2017), “Bayesian registration of functions with a Gaussian process prior,” *Journal of Computational and Graphical Statistics*, 26, 894–904.
- Marron, J. S., Ramsay, J. O., Sangalli, L. M., and Srivastava, A. (2015), “Functional data analysis of amplitude and phase variation,” *Statistical Science*, 468–484.
- Mattar, M. A., Ross, M. G., and Learned-Miller, E. G. (2009), “Nonparametric curve alignment,” in *2009 IEEE International Conference on Acoustics, Speech and Signal Processing*, IEEE, pp. 3457–3460.
- Matuk, J., Bharath, K., Chkrebti, O., and Kurtek, S. (2019), “Bayesian Framework for Simultaneous Registration and Estimation of Noisy, Sparse and Fragmented Functional Data,” *arXiv preprint arXiv:1912.05125*.
- McDonnell, E. I., Zipunnikov, V., Schrack, J. A., Goldsmith, J., and Wrobel, J. (2021), “Registration of 24-hour accelerometric rest-activity profiles and its application to human chronotypes,” *Biological Rhythm Research*, 1–21.

- Müller, M. (2015), *Fundamentals of music processing: Audio, analysis, algorithms, applications*, Springer.
- Nunez, E., Lizarraga, A., and Joshi, S. H. (2021), “SrvfNet: A Generative Network for Unsupervised Multiple Diffeomorphic Functional Alignment,” in *Proceedings of the IEEE/CVF Conference on Computer Vision and Pattern Recognition*, pp. 4481–4489.
- Panaretos, V. M., and Zemel, Y. (2016), “Amplitude and phase variation of point processes,” *The Annals of Statistics*, 44, 771–812.
- Pelties, C., Gabriel, A.-A., and Ampuero, J.-P. (2014), “Verification of an ADER-DG method for complex dynamic rupture problems,” *Geoscientific Model Development*, 847–866.
- Powell, M. J. (2009), “The BOBYQA algorithm for bound constrained optimization without derivatives,” *Cambridge NA Report NA2009/06*, University of Cambridge, Cambridge, 26–46.
- R Core Team (2020), *R: A Language and Environment for Statistical Computing*, R Foundation for Statistical Computing, Vienna, Austria, URL <https://www.R-project.org/>.
- Ramsay, J. O., Graves, S., and Hooker, G. (2020), *fda: Functional Data Analysis*, R package version 5.1.9.
- Ramsay, J. O., and Li, X. (1998), “Curve registration,” *Journal of the Royal Statistical Society: Series B (Statistical Methodology)*, 60, 351–363.
- Ramsay, J. O., and Silverman, B. W. (2005), *Functional Data Analysis*, Springer.
- Rice, J. A., and Wu, C. O. (2001), “Nonparametric mixed effects models for unequally sampled noisy curves,” *Biometrics*, 57, 253–259.
- Sangalli, L. M., Secchi, P., Vantini, S., and Vitelli, V. (2010), “K-mean alignment for curve clustering,” *Computational Statistics & Data Analysis*, 54, 1219–1233.

- Sarkar, S., and Panaretos, V. M. (2021), “CovNet: Covariance Networks for Functional Data on Multidimensional Domains,” *arXiv preprint arXiv:2104.05021*.
- Scheipl, F., Gertheiss, J., Greven, S. et al. (2016a), “Generalized functional additive mixed models,” *Electronic Journal of Statistics*, 10, 1455–1492.
- Scheipl, F., Greven, S. et al. (2016b), “Identifiability in penalized function-on-function regression models,” *Electronic Journal of Statistics*, 10, 495–526.
- Serban, N., Staicu, A.-M., and Carroll, R. J. (2013), “Multilevel cross-dependent binary longitudinal data,” *Biometrics*, 69, 903–913.
- Srivastava, A., Wu, W., Kurtek, S., Klassen, E., and Marron, J. S. (2011), “Registration of functional data using Fisher-Rao metric,” *arXiv preprint arXiv:1103.3817*.
- Stefanucci, M., Sangalli, L. M., and Brutti, P. (2018), “PCA-based discrimination of partially observed functional data, with an application to AneuRisk65 data set,” *Statistica Neerlandica*, 72, 246–264.
- Telesca, D., and Inoue, L. Y. T. (2008), “Bayesian hierarchical curve registration,” *Journal of the American Statistical Association*, 103, 328–339.
- Tipping, M. E., and Bishop, C. M. (1999), “Probabilistic principal component analysis,” *Journal of the Royal Statistical Society: Series B (Statistical Methodology)*, 61, 611–622.
- Tormene, P., Giorgino, T., Quaglini, S., and Stefanelli, M. (2009), “Matching incomplete time series with dynamic time warping: an algorithm and an application to post-stroke rehabilitation,” *Artificial intelligence in medicine*, 45, 11–34.
- Tucker, J. D. (2014), “Functional component analysis and regression using elastic methods,” Ph.D. thesis, The Florida State University.
- (2020), *fdasrvf: Elastic Functional Data Analysis*, R package version 1.9.4.

- Tucker, J. D., Shand, L., and Chowdhary, K. (2021), “Multimodal Bayesian registration of noisy functions using Hamiltonian Monte Carlo,” *Computational Statistics & Data Analysis*, 107298.
- Tucker, J. D., Wu, W., and Srivastava, A. (2013), “Generative models for functional data using phase and amplitude separation,” *Computational Statistics & Data Analysis*, 61, 50–66.
- Uphoff, C., Rettenberger, S., Bader, M., Madden, E. H., Ulrich, T., Wollherr, S., and Gabriel, A.-A. (2017), “Extreme scale multi-physics simulations of the tsunamigenic 2004 sumatra megathrust earthquake,” in *Proceedings of the international conference for high performance computing, networking, storage and analysis*, pp. 1–16.
- van der Linde, A. (2009), “A Bayesian latent variable approach to functional principal components analysis with binary and count data,” *ASTA Advances in Statistical Analysis*, 93, 307–333.
- Vitelli, V. (2019), “A novel framework for joint sparse clustering and alignment of functional data,” *arXiv preprint arXiv:1912.00687*.
- Wagner, H. (2020), *Nonparametric Registration to Low Dimensional Function Spaces*, URL <https://github.com/heikowagner/Nonparametric-Registration-to-Low-Dimensional-Function-Spaces>.
- Wagner, H., and Kneip, A. (2019), “Nonparametric registration to low-dimensional function spaces,” *Computational Statistics & Data Analysis*, 138, 49–63.
- Wang, J.-L., Chiou, J.-M., and Müller, H.-G. (2016), “Functional data analysis,” *Annual Review of Statistics and Its Application*, 3, 257–295.
- Wood, S., and Scheipl, F. (2020), *gamm4: Generalized Additive Mixed Models using 'mgcv' and 'lme4'*, R package version 0.2-6. URL <https://CRAN.R-project.org/package=gamm4>.
- Wood, S. N. (2017), *Generalized additive models: an introduction with R*, CRC press.

- Wood, S. N., Li, Z., Shaddick, G., and Augustin, N. H. (2017), “Generalized additive models for gigadata: modeling the UK black smoke network daily data,” *Journal of the American Statistical Association*, 112, 1199–1210.
- Wrobel, J. (2018), “register: Registration for Exponential Family Functional Data,” *Journal of Open Source Software*, 3, 557.
- Wrobel, J., and Bauer, A. (2021), “registr 2.0: Incomplete Curve Registration for Exponential Family Functional Data,” *Journal of Open Source Software*, 6, 2964.
- Wrobel, J., Muschelli, J., and Leroux, A. (2021), “Diurnal Physical Activity Patterns across Ages in a Large UK Based Cohort: The UK Biobank Study,” *Sensors*, 21, 1545.
- Wrobel, J., Zipunnikov, V., Schrack, J., and Goldsmith, J. (2019), “Registration for exponential family functional data,” *Biometrics*, 75, 48–57.
- Wu, W., and Srivastava, A. (2014), “Analysis of spike train data: Alignment and comparisons using the extended Fisher-Rao metric,” *Electronic Journal of Statistics*, 8, 1776–1785.
- Yao, F., Müller, H.-G., and Wang, J.-L. (2005), “Functional data analysis for sparse longitudinal data,” *Journal of the American statistical association*, 100, 577–590.
- Ypma, J., and Johnson, S. G. (2020), *nloptr*, R package version 1.2.2.2.
- Zhang, A., and Chen, K. (2017), “Nonparametric covariance estimation for mixed longitudinal studies, with applications in midlife women’s health,” *arXiv preprint arXiv:1711.00101*.
- Zhou, L., Huang, J. Z., and Carroll, R. J. (2008), “Joint modelling of paired sparse functional data using principal components,” *Biometrika*, 95, 601–619.

Appendix

A1 Computational Details

We implemented our approach in the package `registr` (Wrobel and Bauer, 2021) for the statistical open-source software R (R Core Team, 2020). The `registr` package allows for the estimation of the joint registration and GFPCA approach both for complete and incomplete curves. All three types of incompleteness (leading, trailing and full incompleteness) and irregular grids are supported. Additional to the methods outlined in this work the package comprises the methods of Wrobel et al. (2019). Several exponential family distributions are available. In the following, we give details on some computational aspects of our method.

A1.1 Registration

The registration codebase builds on the implementation outlined in Wrobel et al. (2019) and Wrobel (2018). We extended the methods by allowing the observed curves to be incomplete. Since the estimation of warping functions in the registration step is performed separately for each curve, we added the option of a parallelized call over the individual curves.

Constrained optimization for the spline coefficients representing the warpings is performed with function `constrOptim()` by inducing linear inequality constraints of the form

$$\mathbf{u}_i \cdot \boldsymbol{\beta}_i - \mathbf{c}_i \geq 0,$$

with parameter vector $\boldsymbol{\beta}_i$ and constraints given by matrix \mathbf{u}_i and vector \mathbf{c}_i . Further details on the constraint matrices are given in Appendix A2. Alternative optimization algorithms

from the NLOpt library (Johnson, 2020) and made available by package `nloptr` (Ypma and Johnson, 2020) were evaluated as well, but did not improve the overall results or lead to a more efficient estimation.

A1.2 Generalized Functional Principal Component Analysis

As outlined in Section 3.2, our adaptation of the two-step GFPCA approach of Gertheiss et al. (2017) is based on an additive regression model with random intercept terms for the individual FPCs. We build on robust and highly efficient software for these kinds of models, available in packages `gamm4` (Wood and Scheipl, 2020) and `lme4` (Bates et al., 2015). The algorithms of `lme4` are highly efficient for estimating models with random intercept terms with several thousand individual categories. The estimation of the marginal mean of the process $X_i(t)$ in the case of very large data with $> 100\,000$ rows is performed with the discretization-based estimation algorithm of function `mgcv::bam` (Wood et al., 2017) rather than the estimation algorithm of `mgcv::gam` (Wood, 2017).

Our implementation of the two-step GFPCA approach of Gertheiss et al. (2017) is based on their accompanying package `gfpc` (Goldsmith, 2016). Additionally we made several adjustments to their codebase to improve overall efficiency: First, while functions `lmer()` and `glmer()` from the `lme4` package default to the optimization routine implemented in function `bobyqa` (package `minqa`, Bates et al., 2014), we make use of the more efficient optimizer `NLOPT_LN_BOBYQA` from the NLOpt library (Johnson, 2020) as described in Powell (2009).

Second, we tackle one major issue in the building of the covariance structure. In principle, the covariance matrix comprises the pairwise covariances between all unique observed time points per functional datum $y_i(t)$. In real data situations with highly irregular grids, the number of unique combinations of time points can explode in size even for settings with a relatively low number of curves. We utilize a binning strategy to handle this problem. Before building the covariance matrix, we round the vector of observed time points to k significant digits. E.g., $k = 3$ then leads to at most 1000^2 unique combinations and a covariance matrix with maximal size 1000×1000 . Similar to the estimation of the marginal

mean of $X_i(t)$, the smoothing of the covariance surface is performed with the discretization-based estimation algorithm `mgcv::bam` rather than `mgcv::gam` if the crossproduct matrix comprises $> 100\,000$ elements.

Third, we updated the codebase of `gamm4` to make the initial construction of the random effect model matrices much more efficient by fully exploiting their sparse structure. Our patched version is currently available on GitHub (<https://github.com/r-gam/gamm4>) and will in future be integrated into the main codebase of the `gamm4` package.

A1.3 Joint approach

To make the overall algorithm more efficient, we introduce two major changes. First, all *intermediate iterations* regarding the GFPCA step, apart from the very first and the very last one, are performed with less accuracy. Above all else, we use larger tolerance values and a simple Laplace approximation to the GLMM likelihood (i.e., `nAGQ = 0` and `nAGQinitStep = FALSE` in function `gamm4::gamm4`) for these iterations. Secondly, we use the solution of the previous GFPCA step as starting values for the subsequent GFPCA step.

A2 Constraint Matrices for `constrOptim()`

As outlined in Appendix A1, we estimate the warping functions using function `constrOptim()`. In the estimation step for one warping function, the parameter vector is constrained s.t. the resulting warping function is monotone and does not exceed the overall time domain $[t_{min}, t_{max}]$.

In the following the constraint matrices are listed for the different settings of (in)completeness and assuming a parameter vector of length p :

$$\boldsymbol{\beta}_i = \begin{pmatrix} \beta_{i1} \\ \beta_{i2} \\ \vdots \\ \beta_{ip} \end{pmatrix} \in \mathbb{R}_{p \times 1}$$

A2.1 Complete curve setting

When all curves were observed completely – i.e. the underlying processes of interest were all observed from the beginning until the end – warping functions can typically be assumed to start and end on the diagonal, since each process is completely observed in its observation interval $[t_{min,i}^*, t_{max,i}^*] \subset [t_{min}, t_{max}]$.

Assuming that both the starting point and the endpoint lie on the diagonal, we set $\beta_{i1} = t_{min,i}^*$ and $\beta_{ip} = t_{max,i}^*$ and only perform the estimation for

$$\begin{pmatrix} \beta_{i2} \\ \beta_{i3} \\ \vdots \\ \beta_{i(p-1)} \end{pmatrix} \in \mathbb{R}_{(p-2) \times 1}$$

This results in the following constraint matrices, that allow a mapping from the observed domain $[t_{min,i}^*, t_{max,i}^*]$ to the domain itself $[t_{min,i}^*, t_{max,i}^*] \subset [t_{min}, t_{max}]$:

$$\mathbf{u}_i = \begin{pmatrix} 1 & 0 & 0 & 0 & \dots & 0 & 0 & 0 \\ -1 & 1 & 0 & 0 & \dots & 0 & 0 & 0 \\ 0 & -1 & 1 & 0 & \dots & 0 & 0 & 0 \\ \vdots & \ddots \\ 0 & 0 & 0 & 0 & \dots & 0 & -1 & 1 \\ 0 & 0 & 0 & 0 & \dots & 0 & 0 & -1 \end{pmatrix} \in \mathbb{R}_{(p-1) \times (p-2)}$$

$$\mathbf{c}_i = \begin{pmatrix} t_{min,i}^* \\ 0 \\ 0 \\ \vdots \\ 0 \\ -1 \cdot t_{max,i}^* \end{pmatrix} \in \mathbb{R}_{(p-1) \times 1}$$

A2.2 Leading incompleteness only

In the case of leading incompleteness – i.e. the underlying processes of interest were all observed until their very end but not necessarily starting from their beginning – warping

functions can typically be assumed to end on the diagonal, s.t. one assumes $\beta_{ip} = t_{max,i}^*$ to let the warping functions end at the last observed time point $t_{max,i}^*$. The estimation is then performed for the remaining parameter vector

$$\begin{pmatrix} \beta_{i1} \\ \beta_{i3} \\ \vdots \\ \beta_{i(p-1)} \end{pmatrix} \in \mathbb{R}_{(p-1) \times 1}$$

This results in the following constraint matrices, that allow a mapping from the observed domain $[t_{min,i}^*, t_{max,i}^*]$ to the domain $[t_{min}, t_{max,i}^*] \subset [t_{min}, t_{max}]$:

$$\mathbf{u}_i = \begin{pmatrix} 1 & 0 & 0 & 0 & \dots & 0 & 0 & 0 \\ -1 & 1 & 0 & 0 & \dots & 0 & 0 & 0 \\ 0 & -1 & 1 & 0 & \dots & 0 & 0 & 0 \\ \vdots & \ddots \\ 0 & 0 & 0 & 0 & \dots & 0 & -1 & 1 \\ 0 & 0 & 0 & 0 & \dots & 0 & 0 & -1 \end{pmatrix} \in \mathbb{R}_{p \times (p-1)}$$

$$\mathbf{c}_i = \begin{pmatrix} t_{min} \\ 0 \\ 0 \\ \vdots \\ 0 \\ -1 \cdot t_{max,i}^* \end{pmatrix} \in \mathbb{R}_{p \times 1}$$

A2.3 Trailing incompleteness only

In the case of trailing incompleteness – i.e. the underlying processes of interest were all observed from the beginning but not necessarily until their very end – warping functions can typically be assumed to start on the diagonal, s.t. one assumes $\beta_{i1} = t_{min,i}^*$ to let the warping functions start at the first observed time point $t_{min,i}^*$. The estimation is then

performed for the remaining parameter vector

$$\begin{pmatrix} \beta_{i2} \\ \beta_{i3} \\ \vdots \\ \beta_{ip} \end{pmatrix} \in \mathbb{R}_{(p-1) \times 1}$$

This results in the following constraint matrices, that allow a mapping from the observed domain $[t_{min,i}^*, t_{max,i}^*]$ to the domain $[t_{min,i}^*, t_{max}] \subset [t_{min}, t_{max}]$:

\mathbf{u}_i identical to the version for leading incompleteness

$$\mathbf{c}_i = \begin{pmatrix} t_{min,i}^* \\ 0 \\ 0 \\ \vdots \\ 0 \\ -1 \cdot t_{max} \end{pmatrix} \in \mathbb{R}_{p \times 1}$$

A2.4 Leading and trailing incompleteness

In the case of both leading and trailing incompleteness – i.e. the underlying processes of interest were neither necessarily observed from their very beginnings nor to their very ends – warping functions can typically only be assumed to map the observed domains $[t_{min,i}^*, t_{max,i}^*]$ to the overall domain $[t_{min}, t_{max}]$.

This results in the following constraint matrices:

$$\mathbf{u}_i = \begin{pmatrix} 1 & 0 & 0 & 0 & \dots & 0 & 0 & 0 \\ -1 & 1 & 0 & 0 & \dots & 0 & 0 & 0 \\ 0 & -1 & 1 & 0 & \dots & 0 & 0 & 0 \\ \vdots & \ddots \\ 0 & 0 & 0 & 0 & \dots & 0 & -1 & 1 \\ 0 & 0 & 0 & 0 & \dots & 0 & 0 & -1 \end{pmatrix} \in \mathbb{R}_{(p+1) \times p}$$

$$\mathbf{c}_i = \begin{pmatrix} t_{min} \\ 0 \\ 0 \\ \vdots \\ 0 \\ -1 \cdot t_{max} \end{pmatrix} \in \mathbb{R}_{(p+1) \times 1}$$

A3 Simulation study

A3.1 Simulation setting

This subsection contains figures for all relevant components of the curves simulated in the simulation study.

A3.1.1 Distribution of the data

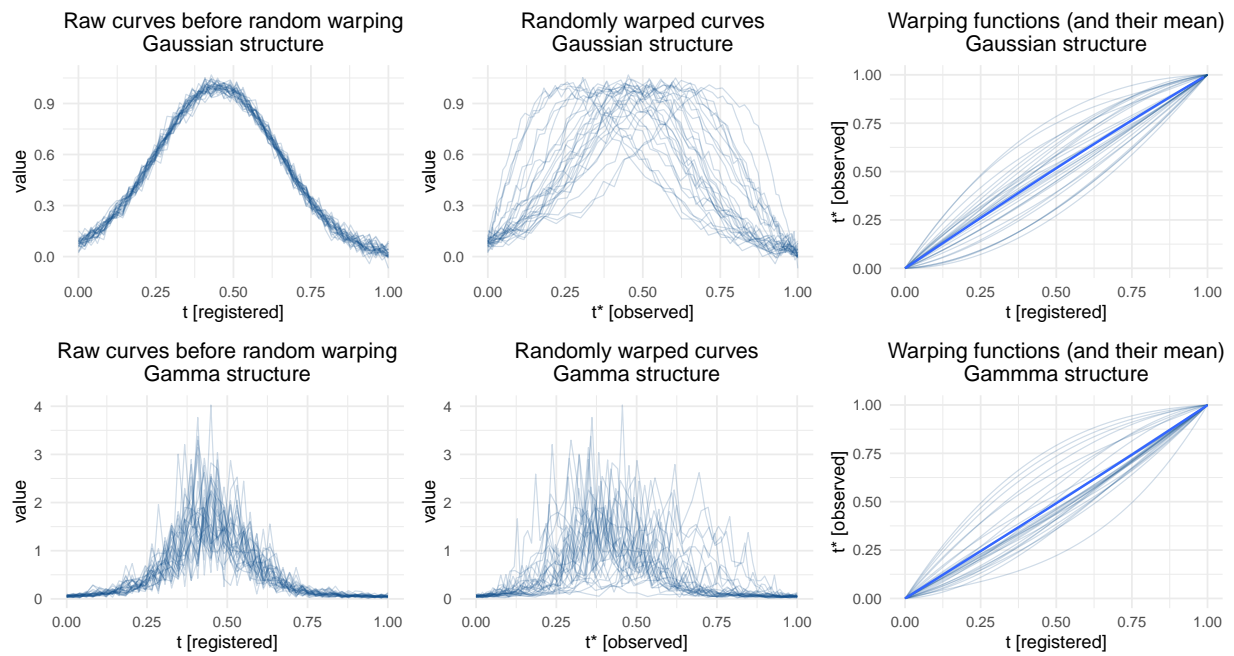


Figure 9: Structure of simulated Gaussian and Gamma data (top and bottom row, respectively), before adding amplitude variation

A3.1.2 Rank of amplitude variation

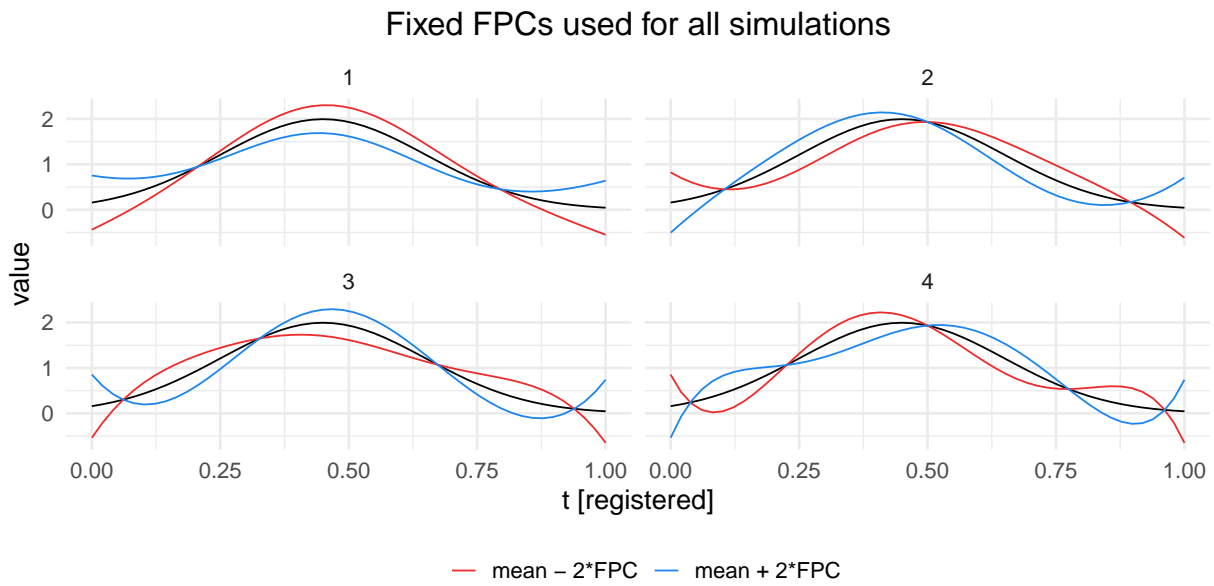


Figure 10: Simulated eigenfunctions / functional principal components (FPCs), visualized by adding and subtracting them from a some mean curve (black line)

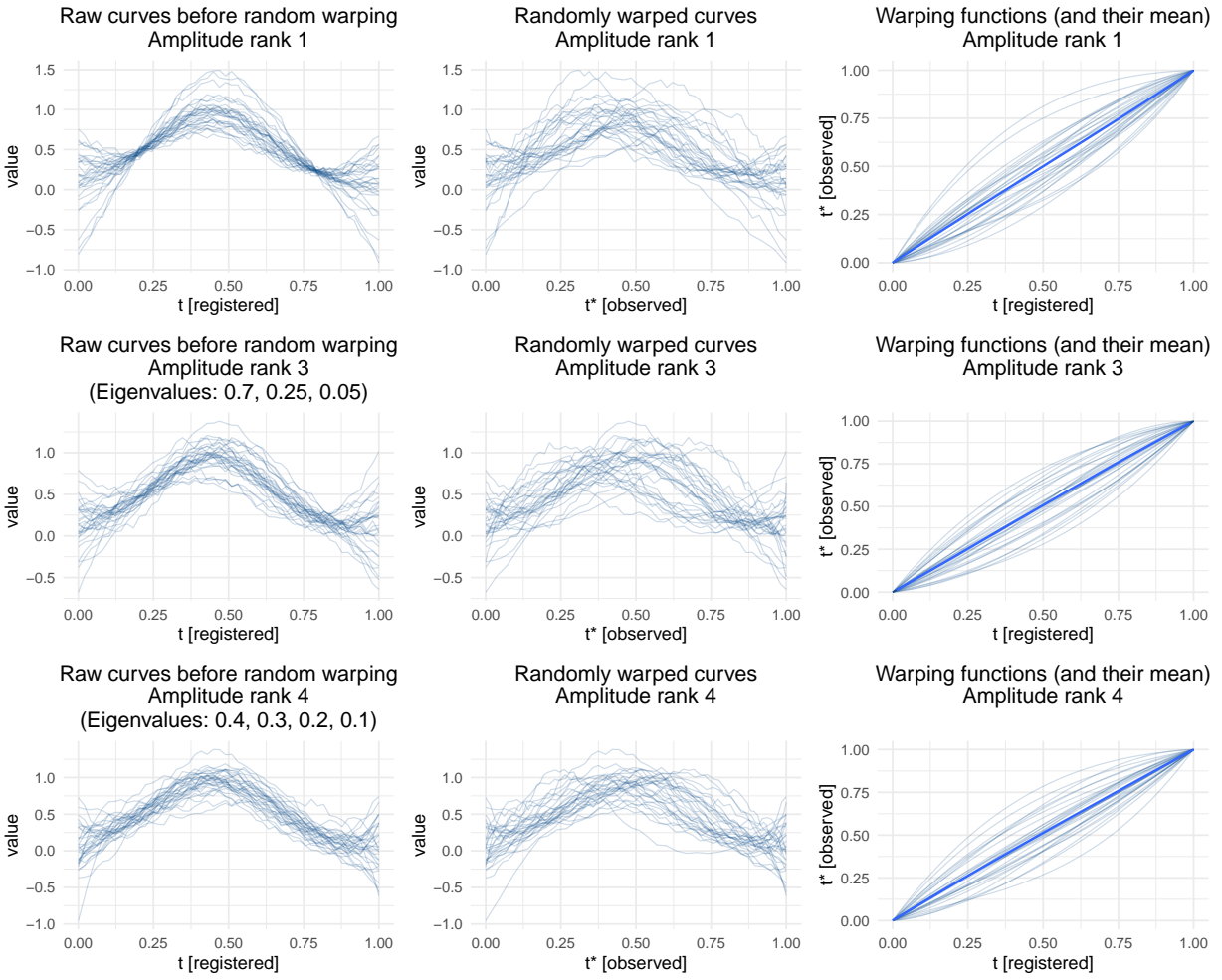


Figure 11: Simulated curves with Gaussian structure, including amplitude variation and random warping.

A3.1.3 Strength of incompleteness

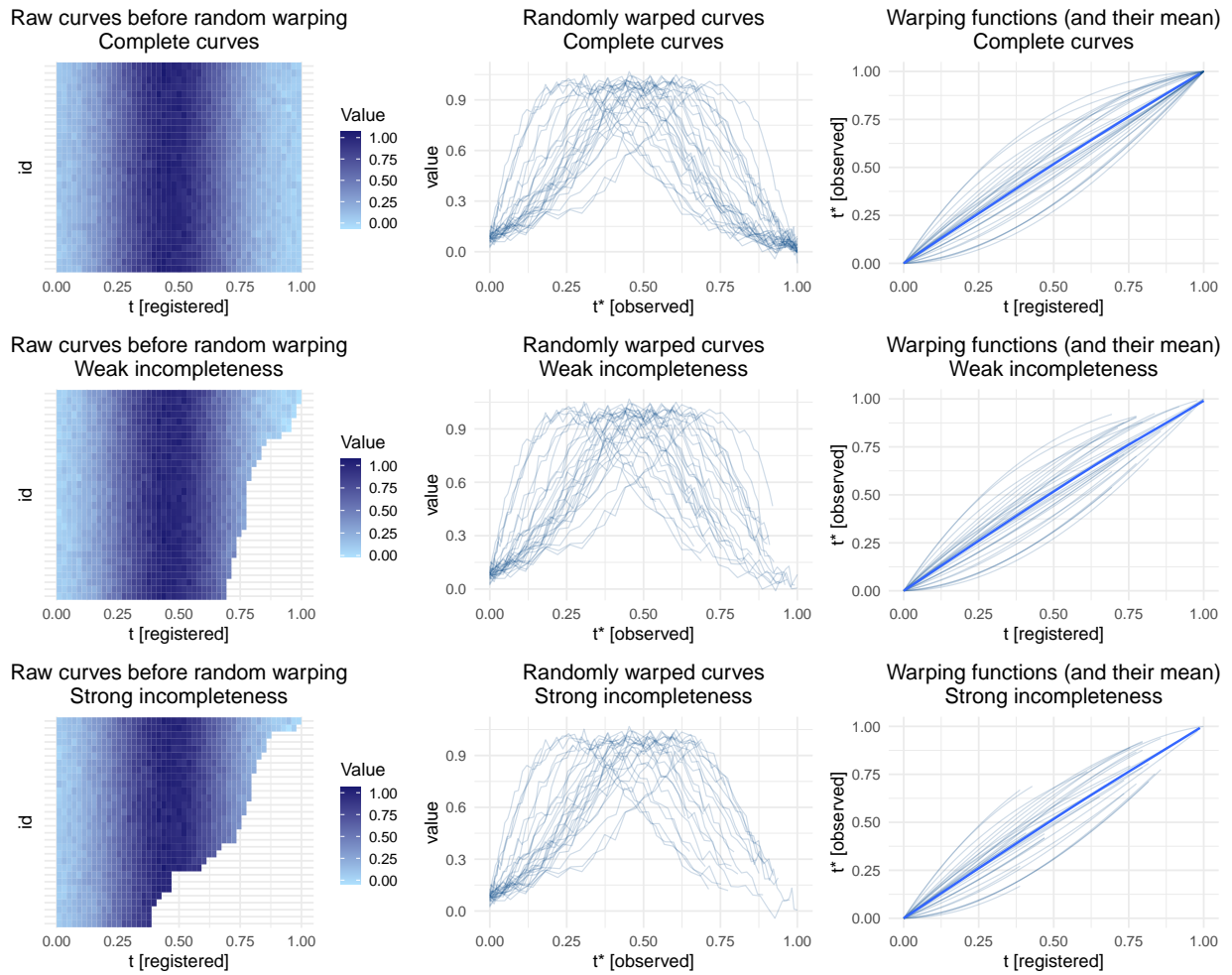


Figure 12: Simulated curves with Gaussian structure and different strengths of incompleteness.

A3.1.4 Correlation structure

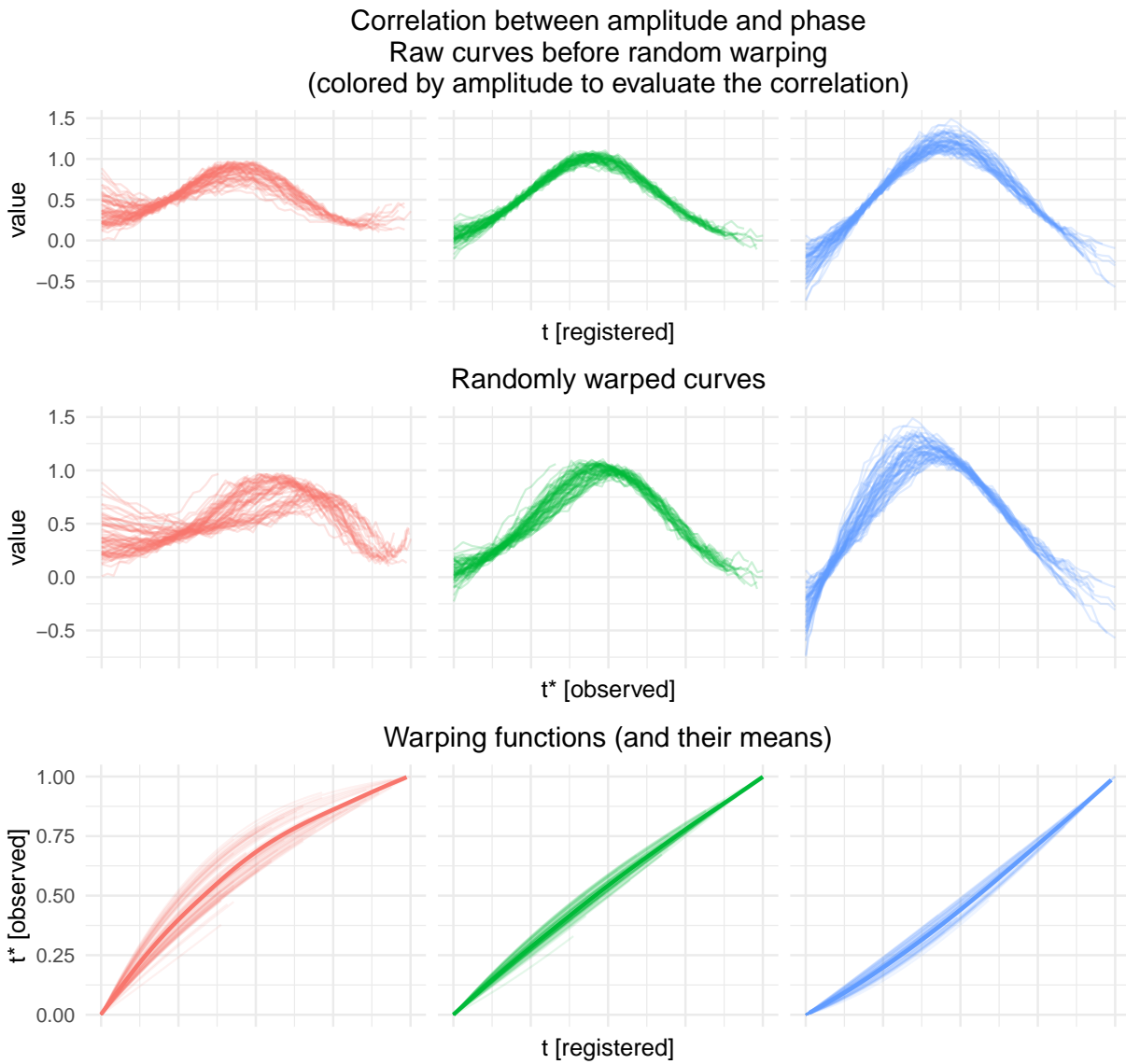


Figure 13: Simulated curves with Gaussian structure and correlated amplitude and phase variation.

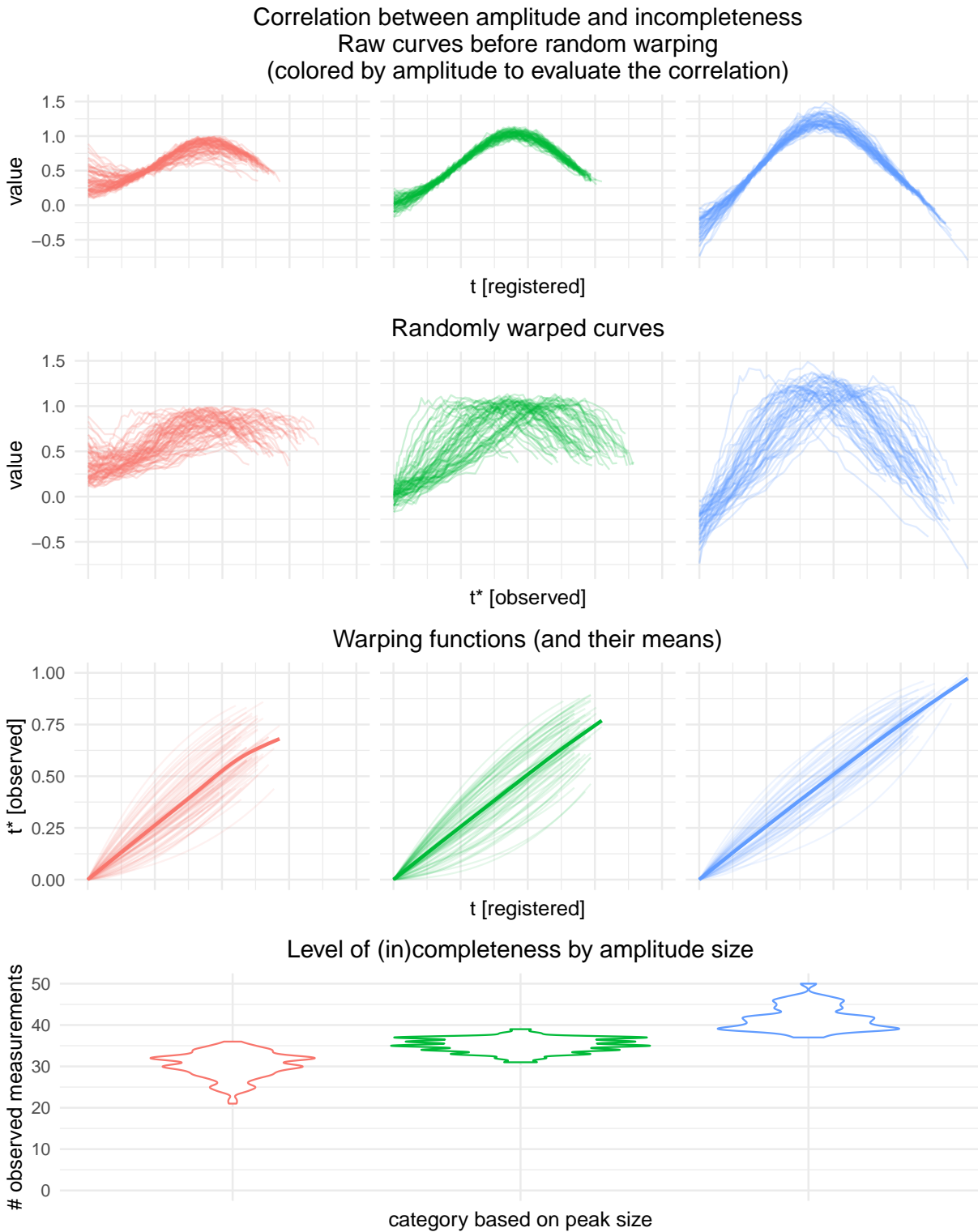


Figure 14: Simulated curves with Gaussian structure and correlated amplitude variation and amount of incompleteness.

A3.2 Simulation results – Gaussian with correlation structure

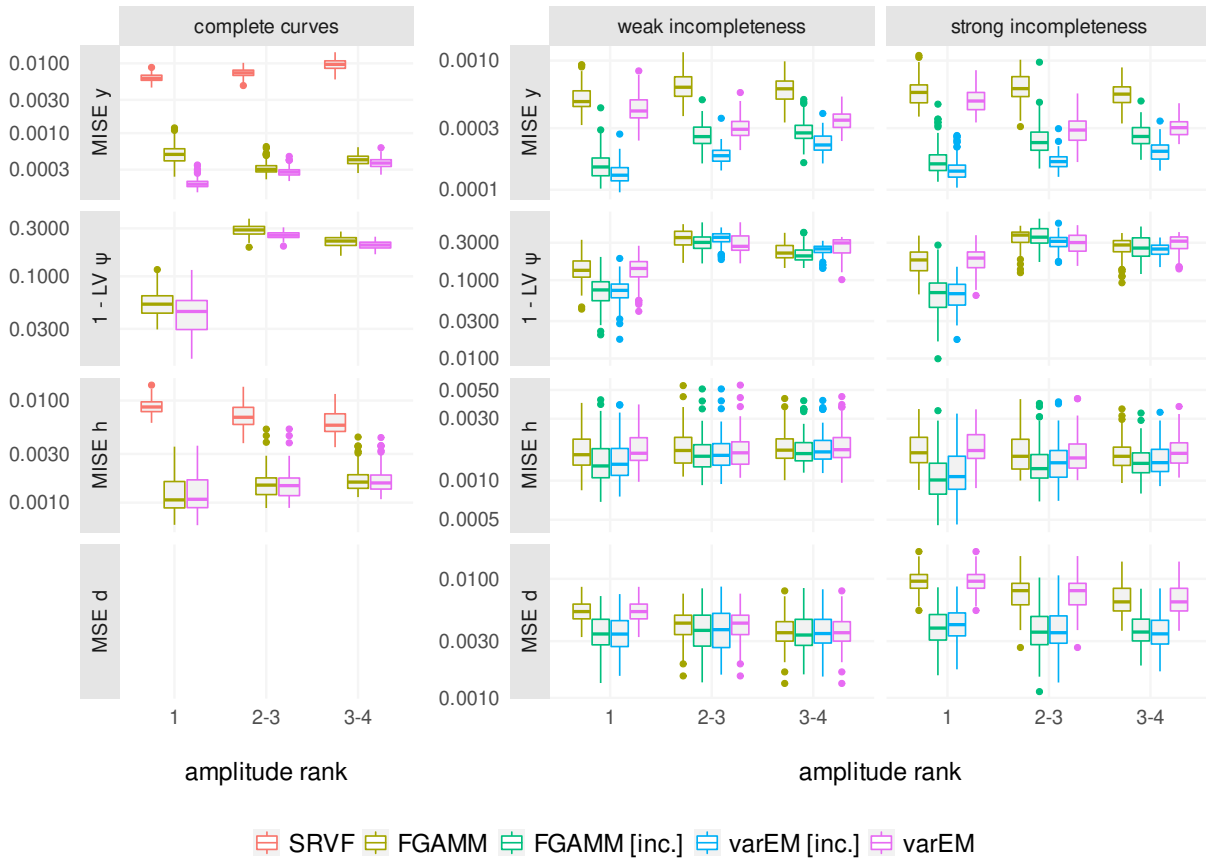


Figure 15: Results for the simulation setting with Gaussian data and a correlation between amplitude and phase.

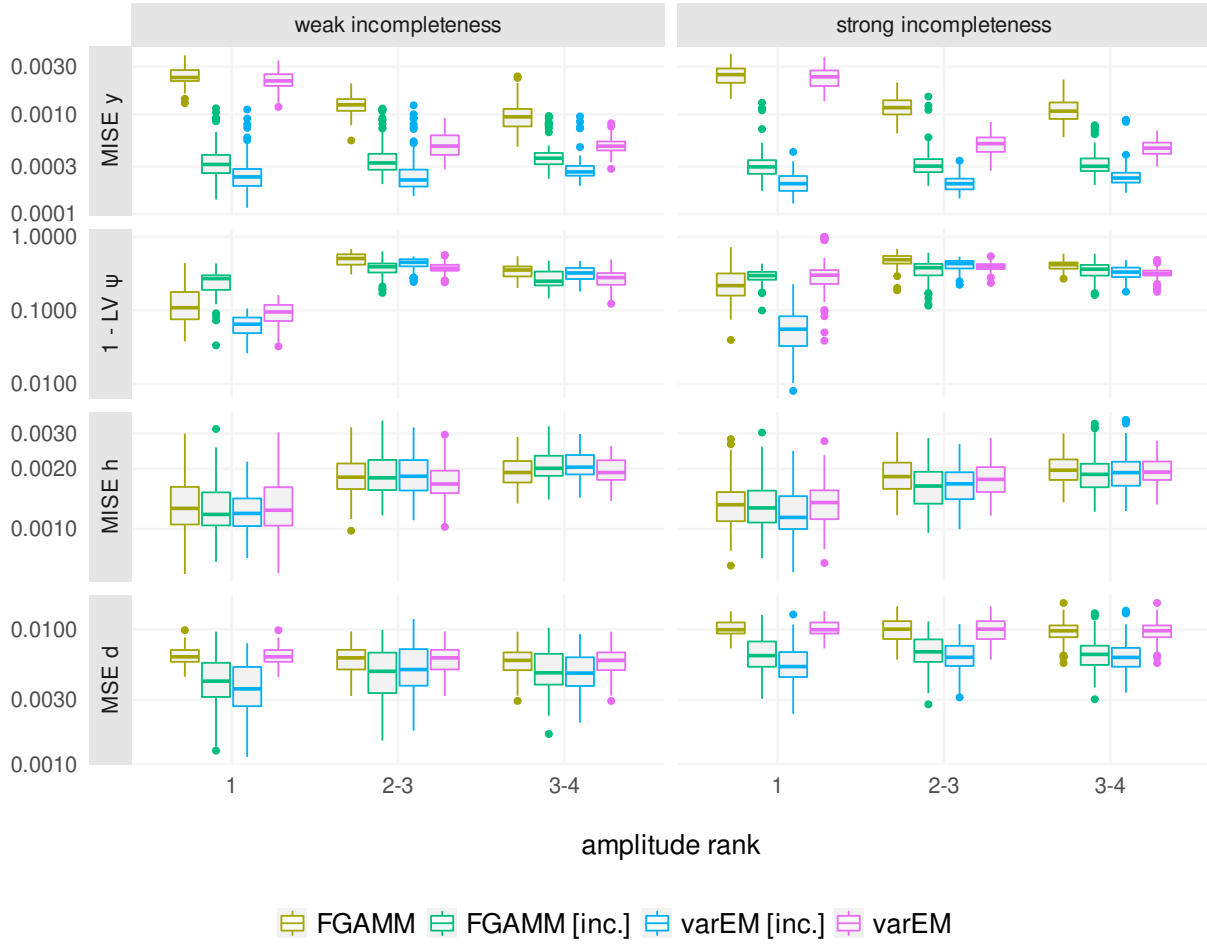


Figure 16: Results for the simulation setting with Gaussian data and a correlation between amplitude and the amount of incompleteness.

A3.3 Simulation results – Gamma with correlation structure

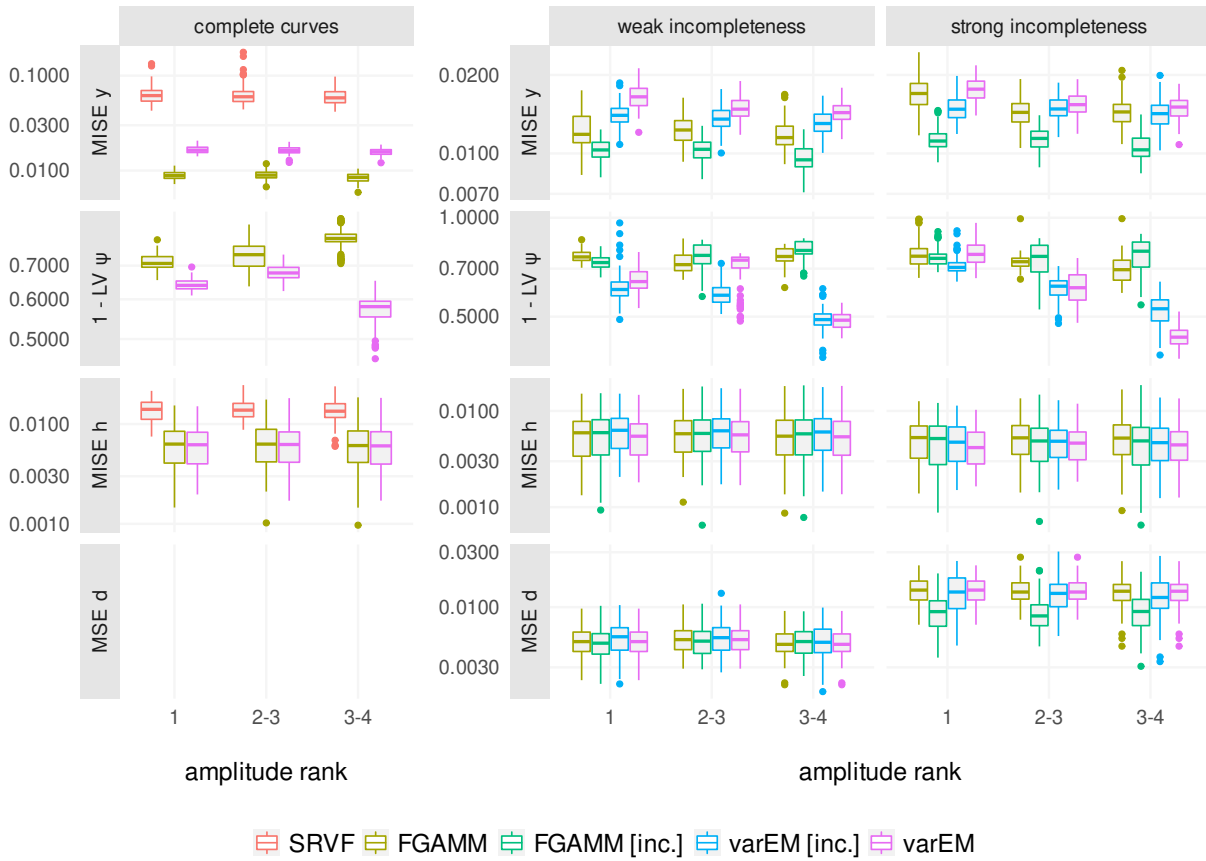


Figure 17: Results for the simulation setting with Gamma data and a correlation between amplitude and phase.

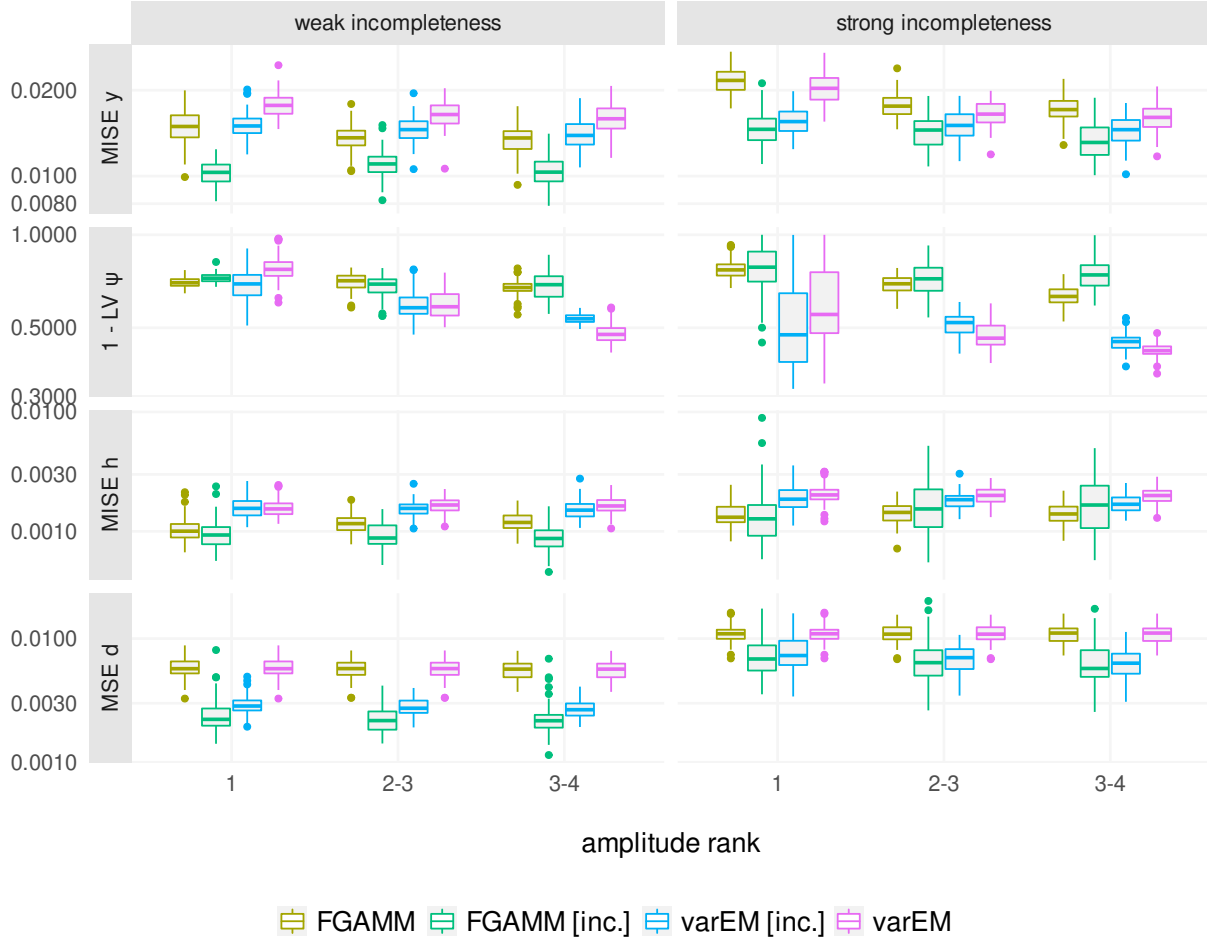


Figure 18: Results for the simulation setting with Gamma data and a correlation between amplitude and the amount of incompleteness.

A3.4 Simulation results – Gaussian with adaptive FPC estimation

In contrast to the previous settings of the simulation study, the number of Functional Principal Components (FPCs) in the following settings is not fixed to the simulated rank of amplitude variation. Instead, in each iterative FPCA step (i) the varEM approach uses as many FPCs as are needed to explain 90% of the overall amplitude variation, and (ii) the FGAMM approach uses as many FPCs as are needed to explain 90% of the overall amplitude variation, while dropping such FPCs that explain $< 2\%$ of the variation (see

criterion outlined at the end of Section 3).

For the varEM approach, the explained share of variance and accordingly the number of FPCs in each iteration is estimated before the main iteration's estimation step by once running the FPCA with 20 FPCs and correspondingly 20 B-spline basis functions to represent the FPC basis. Doing so, we approximate the overall variance in the varEM approach with the variance represented by this FPC basis with 20 FPCs. In contrast to the simulation results in the main part of our paper, we accordingly use 20 instead of eight basis functions for the estimation of the FPC basis in the varEM approach.

Note that the third and fourth FPC in the simulation settings with amplitude rank 2–3 and 3–4 only explain 5% and 10% of the overall amplitude variation, respectively (see Section 4.1). Accordingly, it is not unreasonable if fewer than 3 and 4 FPCs are chosen based on the $\geq 90\%$ criterion, respectively.

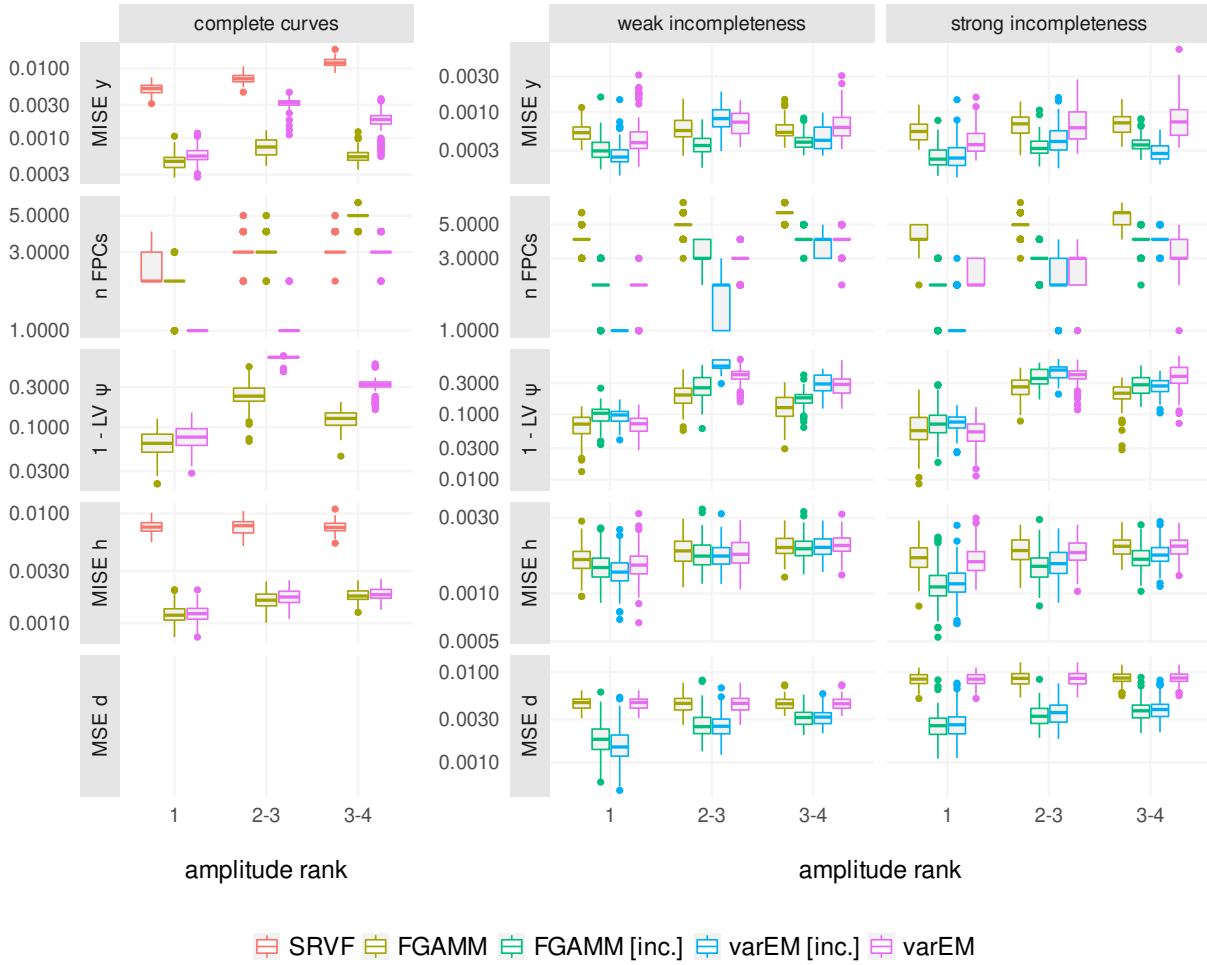


Figure 19: Results for the simulation setting with Gaussian data and mutually uncorrelated amplitude, phase and amount of incompleteness, where the number of FPCs was adaptively estimated. All y scales are \log_{10} transformed.

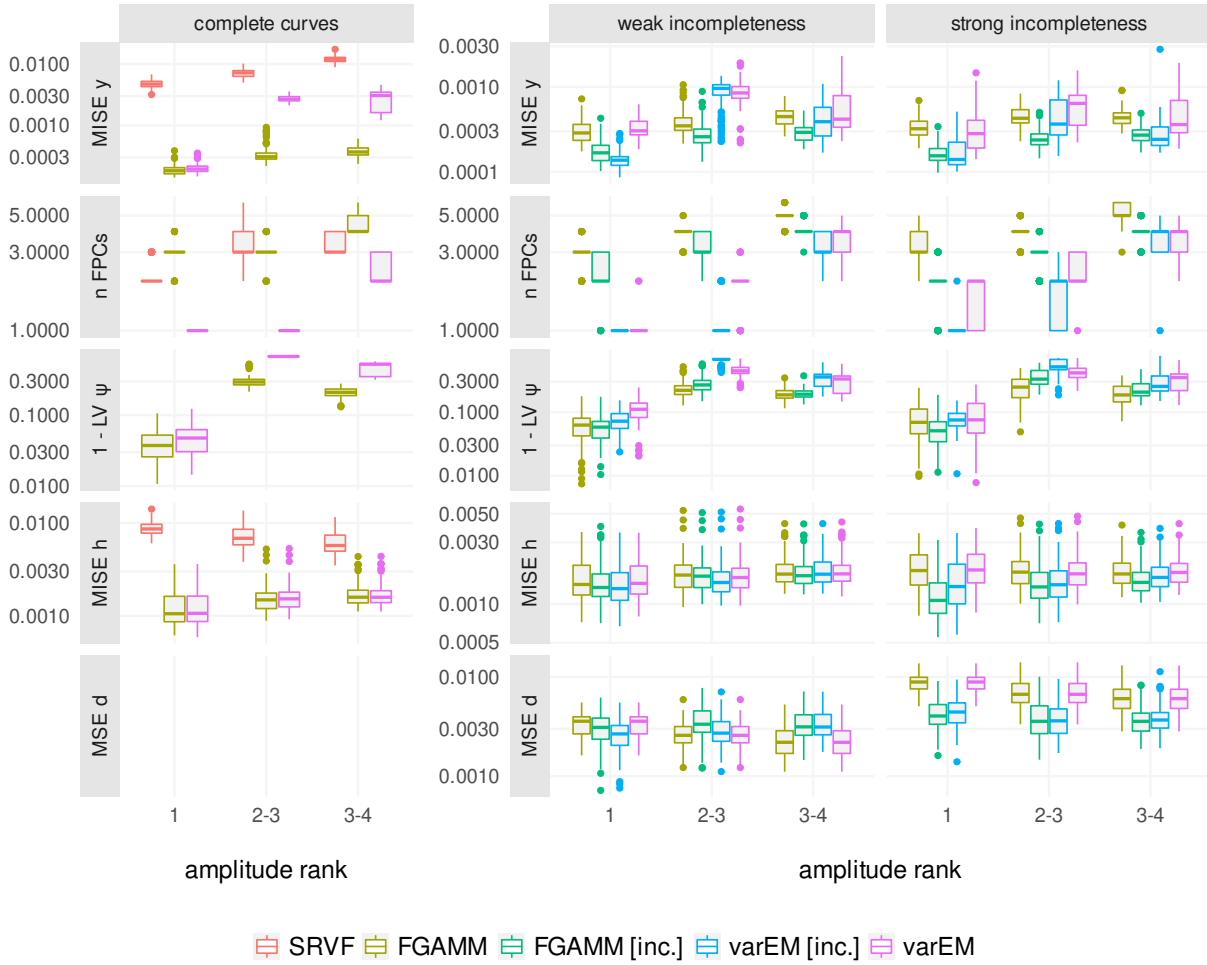


Figure 20: Results for the simulation setting with Gaussian data and a correlation between amplitude and phase, where the number of FPCs was adaptively estimated.

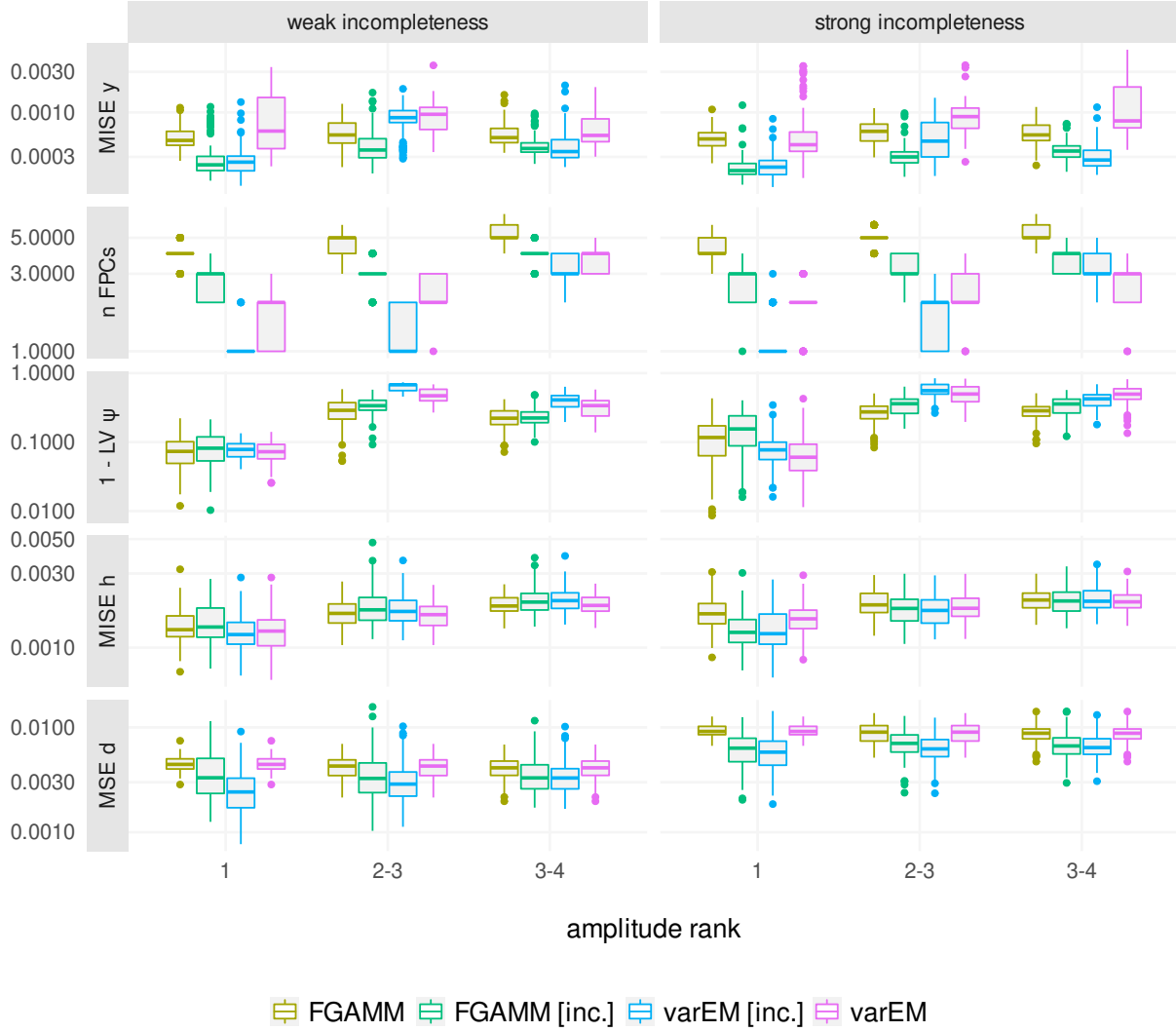


Figure 21: Results for the simulation setting with Gaussian data and a correlation between amplitude and the amount of incompleteness, where the number of FPCs was adaptively estimated.

A3.5 Simulation results – Gamma with adaptive FPC estimation

Note our remarks at the beginning of Appendix A3.4. The only difference to the Gaussian setting is that the FGAMM approach assumes a Gamma distribution instead of a Gaussian structure.

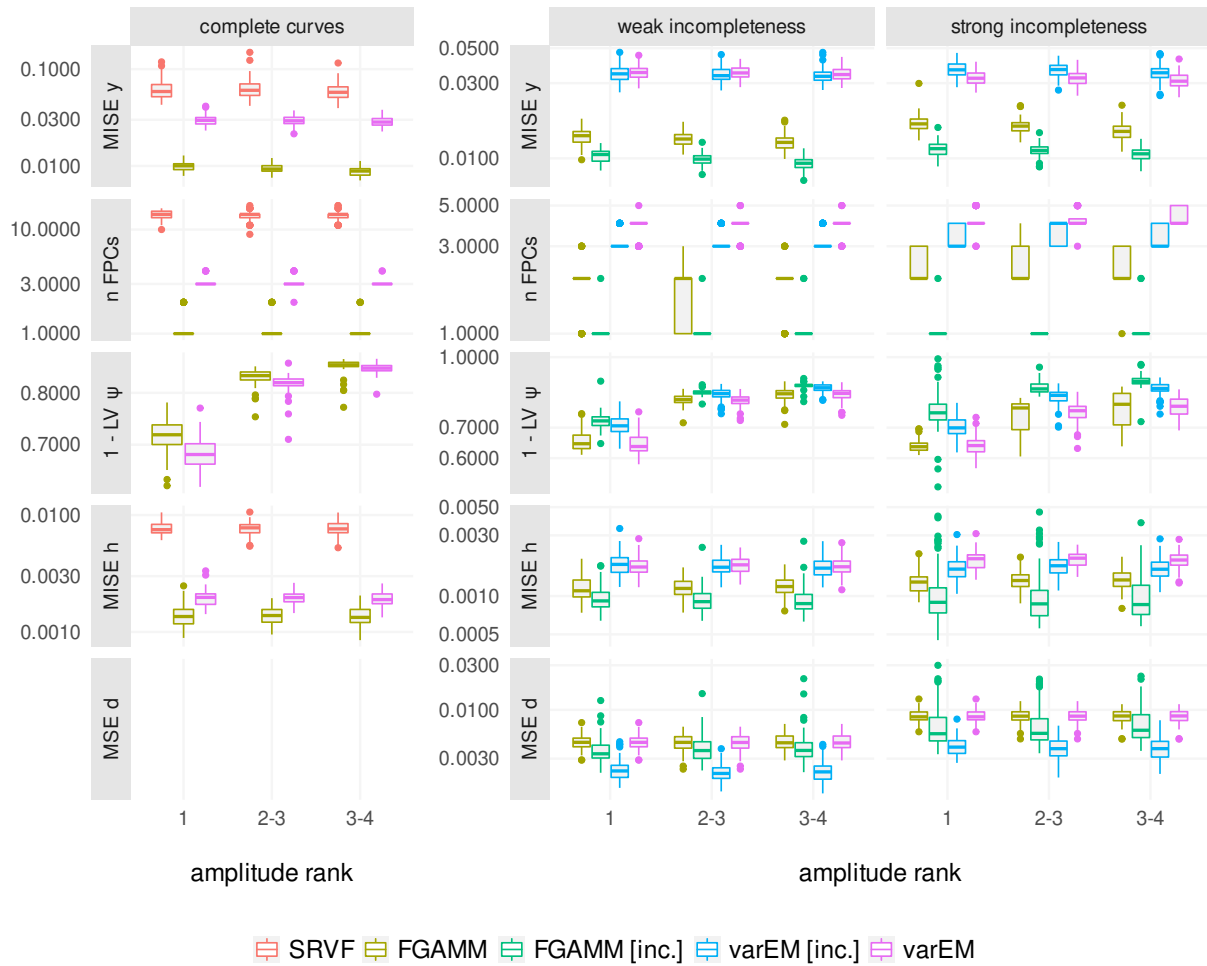


Figure 22: Results for the simulation setting with Gamma data and mutually uncorrelated amplitude, phase and amount of incompleteness, where the number of FPCs was adaptively estimated.

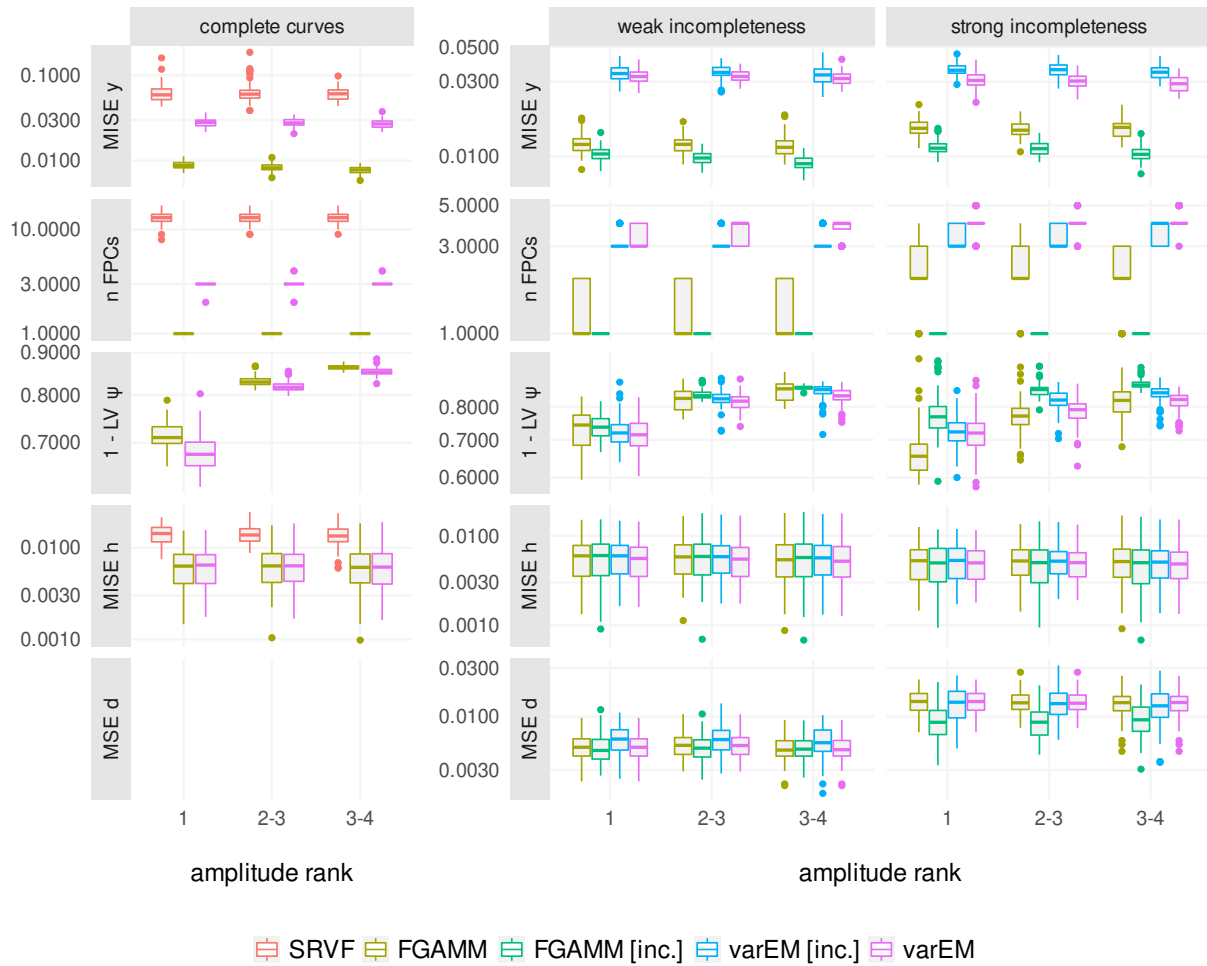


Figure 23: Results for the simulation setting with Gamma data and a correlation between amplitude and phase, where the number of FPCs was adaptively estimated.

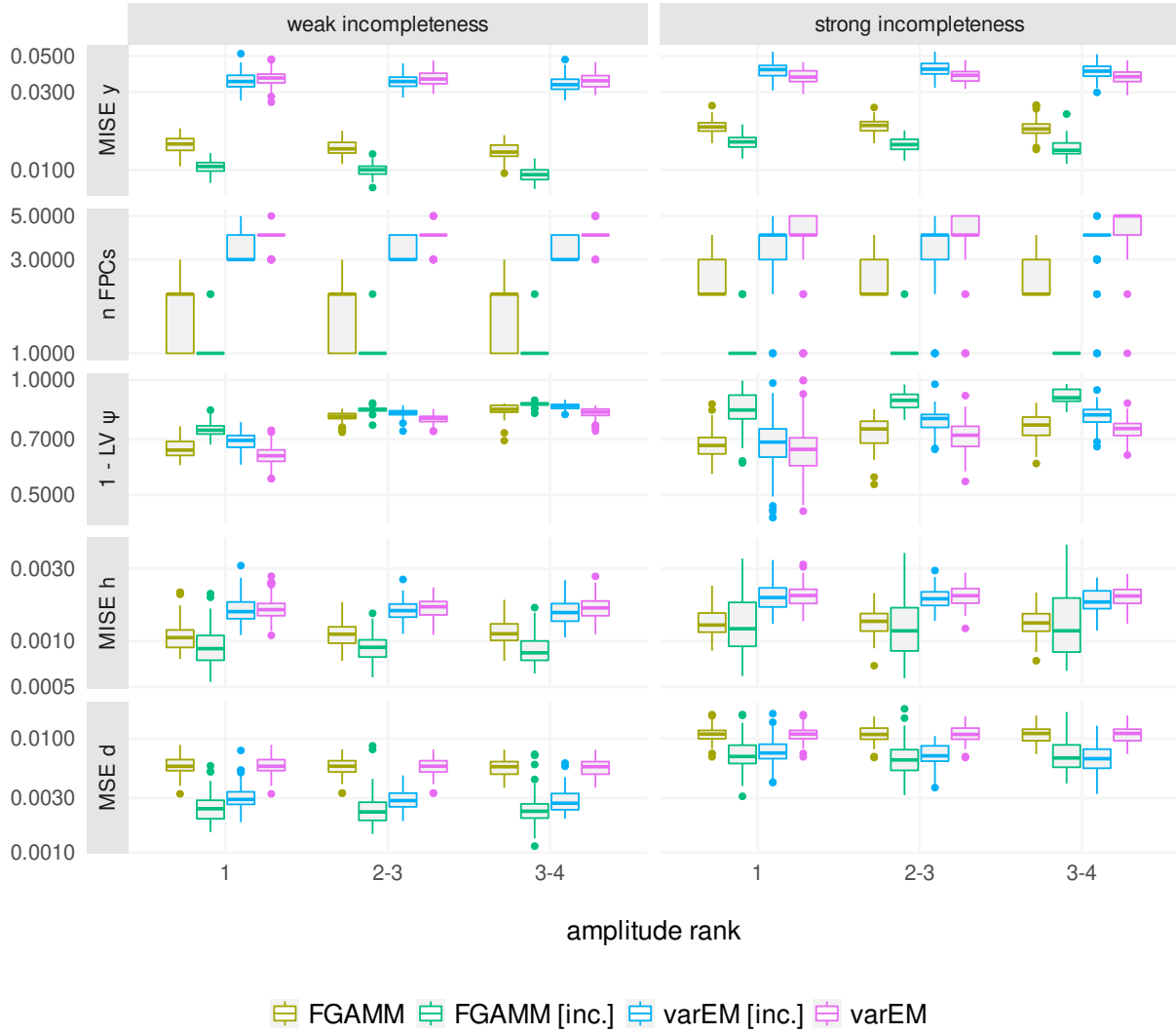


Figure 24: Results for the simulation setting with Gamma data and a correlation between amplitude and the amount of incompleteness, where the number of FPCs was adaptively estimated.

A4 Berkeley application

A4.1 Curves with simulated incompleteness

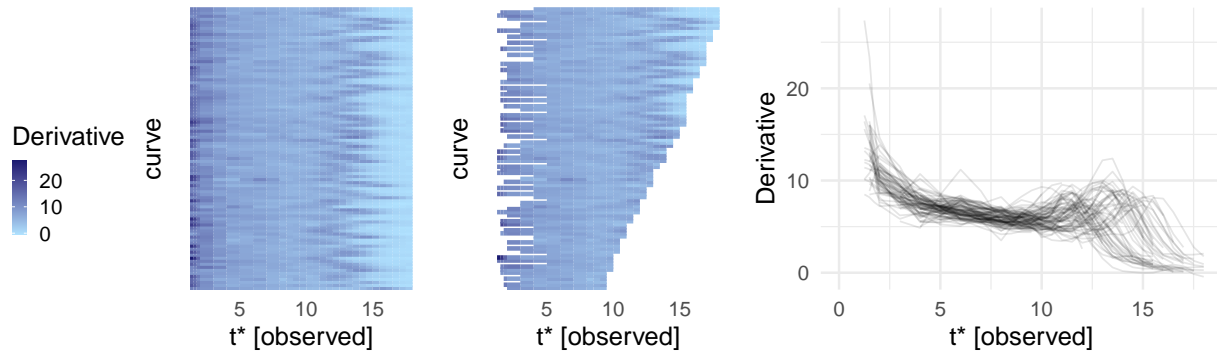


Figure 25: Lasagna plot of observed curves (left pane) and curves with simulated incompleteness (right) for the first derivative of the Berkeley child growth data.

A4.2 Detailed results

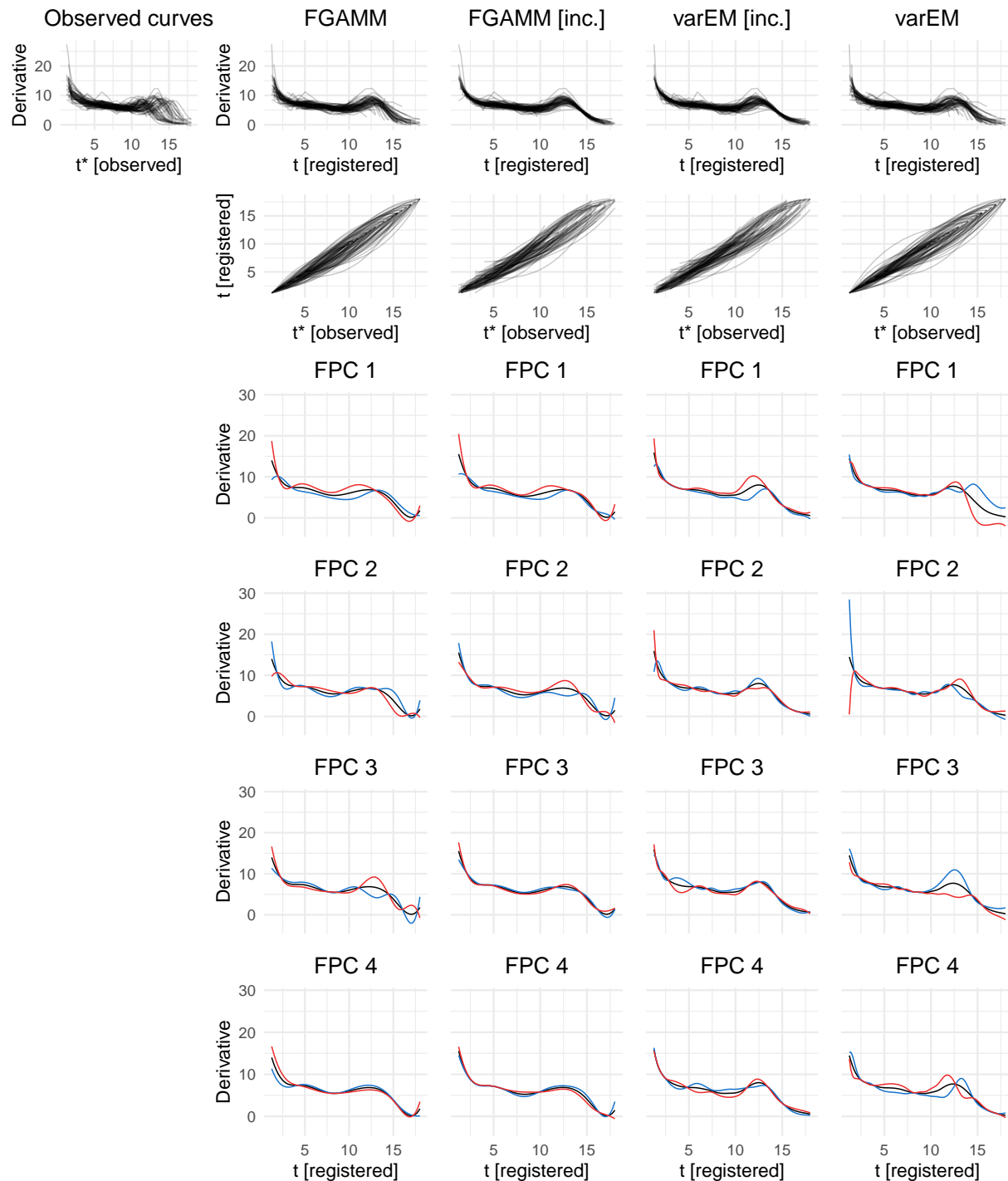


Figure 26: Observed curves (top left pane), registered curves (top row), estimated inverse warping functions (second row) and the first four estimated FPCs based on the different approaches. The FPCs $\psi_k(t)$ are visualized by displaying the overall mean curve (solid line) plus (dashed line, $+$) and minus (dotted line, $-$) $x \cdot \psi_k(t)$, with x twice the standard deviation of the individual FPC's scores.

A4.3 Varying the penalization parameter λ

The results based on different λ values are shown in Figure 27. The example is based on the Berkeley data discussed in Section 5.

While the overall domain dilation of the warping functions is not penalized with $\lambda = 0$, this is the case the higher the penalization parameter λ is chosen. With value $\lambda = 1$ the penalization is strong enough to cause all registered domain lengths to be (quasi) identical to the observed domain lengths.

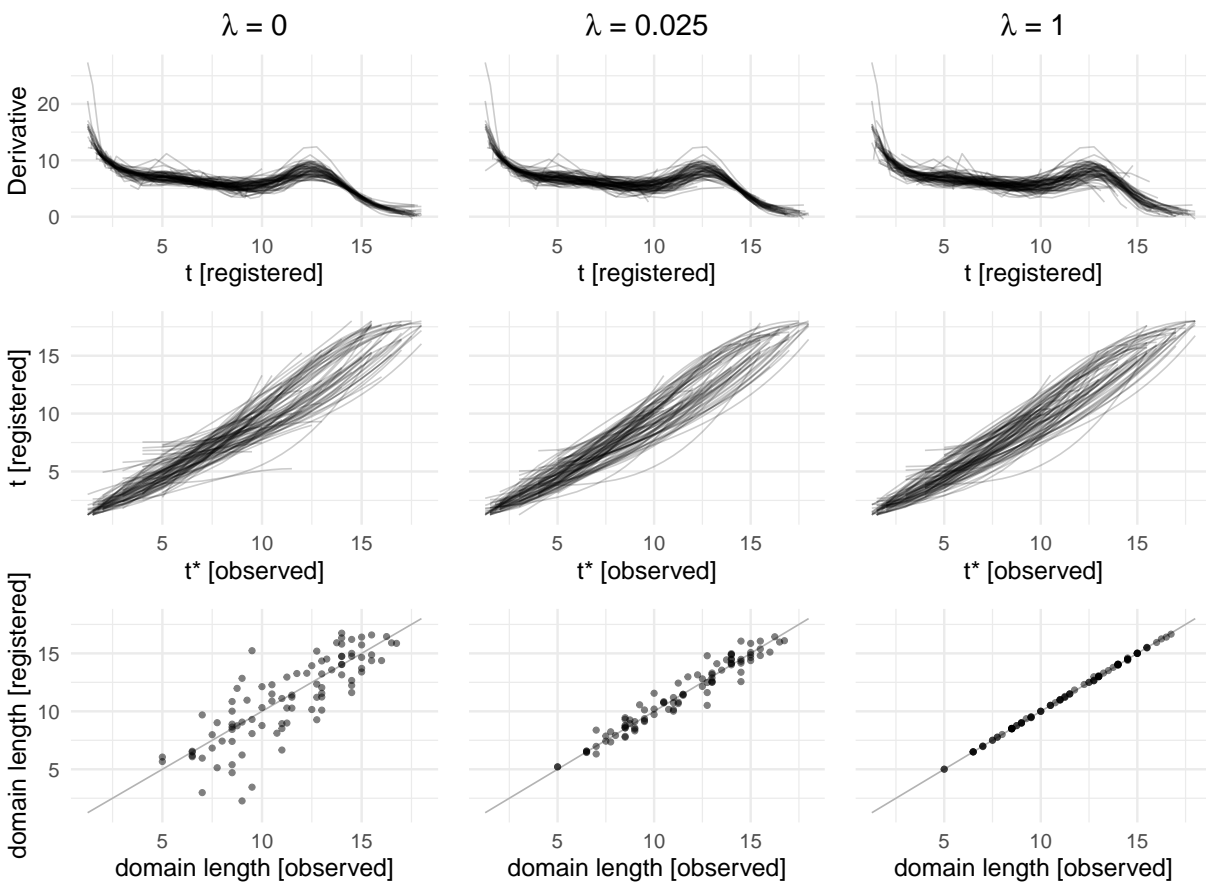


Figure 27: Results for varying values of the penalization parameter λ after joint registration and Gaussian FPCA with the FGAMM approach. The graphic shows spaghetti plots of the registered curves (first row), estimated warping functions (second row) and the difference between the observed domain lengths and the registered domain lengths (bottom row).

A5 Seismic application

A5.1 Estimated inverse warping functions

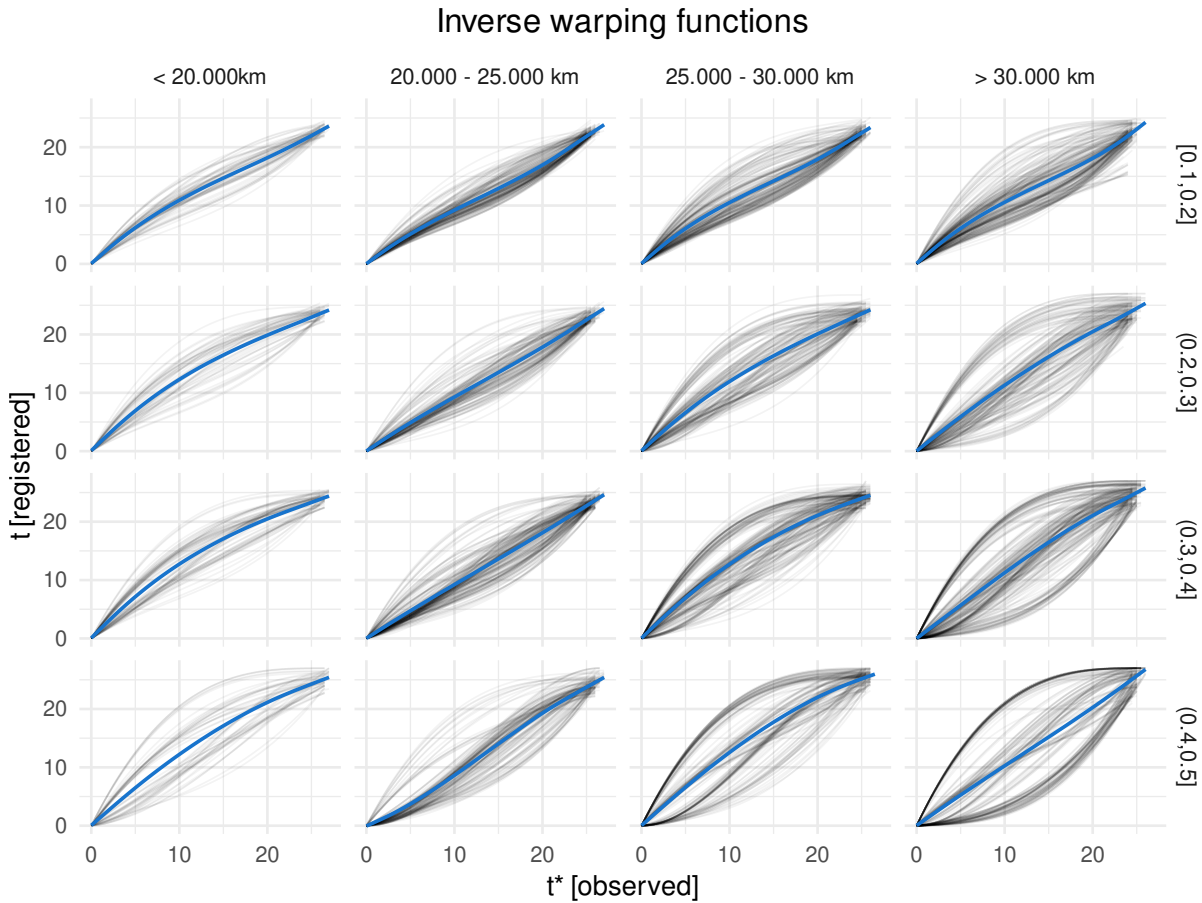


Figure 28: Estimated inverse warping functions displayed against the hypocentral distance of the seismometers (x-axis) and the dynamic coefficient of friction μ_d (y-axis). In each panel, a solid blue curve marks the mean curve based on all respective warping functions.

A5.2 Estimated phase and amplitude variation over space

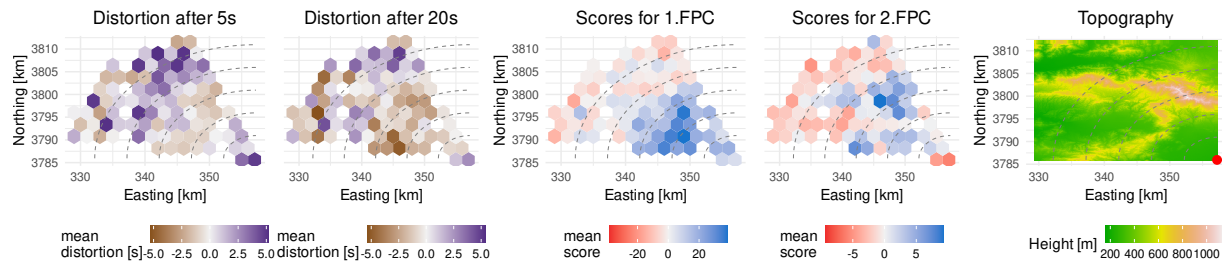


Figure 29: Estimated phase and amplitude variation visualized over the evaluated region. Phase variation and amplitude variation are shown by displaying the mean of the overall time distortion after 5 and 20 seconds (left pane, with positive and negative values representing time dilation and compression, respectively) and of the curves’ mean scores for the FPCs, respectively. The right plot shows the topography of the region, with the epicenter marked as red dot. The grey dashed lines mark the distance to the epicenter in 5km steps.

A6 GFPCA: Structure of subordinate FPCs

This section evaluates one Gaussian data setting from the simulation study to showcase the issue of subordinate functional principal components (FPCs) which

1. individually explain a very small share of the overall amplitude variation, but jointly explain a relevant share, and
2. often tend to represent phase variation rather than amplitude variation.

For this evaluation, 100 curves are simulated similarly to the simulation setting with complete curves, Gaussian noise, amplitude rank 2–3 and no correlation between amplitude variation and phase variation. The only differences to the simulation study are the following:

- the curves are not randomly warped,

- a regular time grid with length 100 is used.

The simulated curves are visualized in Figure 30. We estimate a solution with 20 FPCs with the two-step approach. These first 20 FPCs and their explained shares of variance are visualized in Figure 31.

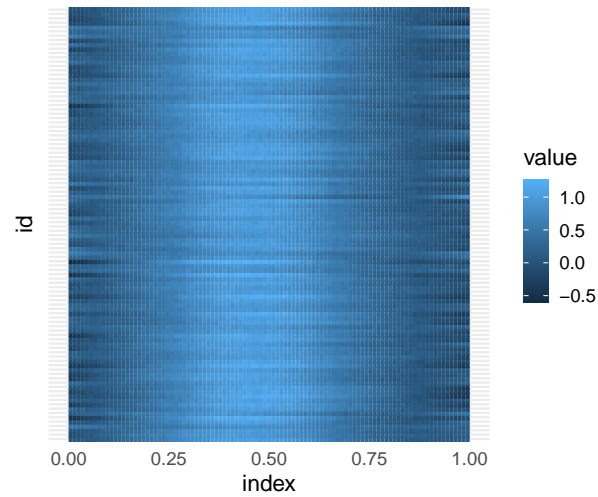


Figure 30: Lasagna plot of the simulated curves.



Figure 31: Visualization of the first 20 FPCs including their percentage of explained variance (PVE).

A7 Choosing the initial template function

To check how much the results of the joint registration and GFPCA approach vary based on different template functions for the initial registration step, we run the application on the Berkeley data (from Section 5.1) with four different template functions:

- Template 1: Overall mean curve (similar to the application in the main paper)
- Template 2: Curve where the main peak in the second half of the domain is not very salient and occurs quite early on
- Template 3: Curve where the main peak occurs a bit later on and is a bit more salient

- Template 4: Curve where the main peak is even more salient

The template functions and the results of the application of the FGAMM approach to the data can be found in the following Figure.

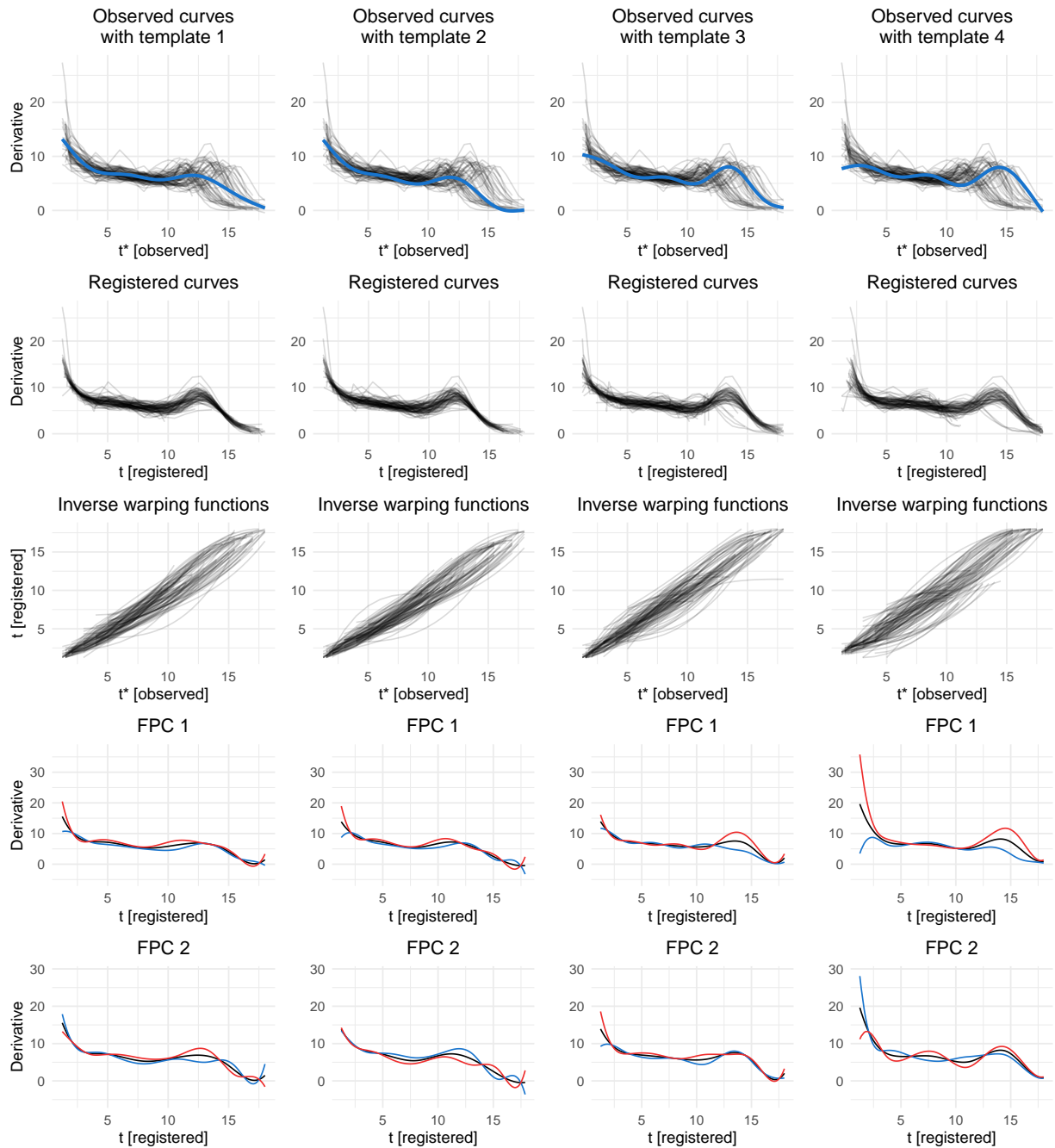


Figure 32: Results of the FGAMM approach based on the different initial template functions (one column per template function). The rows contain the observed curves with the template function in blue (first row), the registered curves (second row), the estimated inverse warping functions (third row) and the first two estimated FPCs (last two rows). The FPCs $\psi_k(t)$ are visualized by the overall mean curve (solid line) plus (blue line) and minus (red line) $2 \cdot \sqrt{\hat{\tau}_k} \cdot \psi_k(t)$, with $\sqrt{\hat{\tau}_k}$ the standard deviation of the estimated scores for the k 'th FPC.